DESIGN, DEVELOPMENT, AND FUNCTIONAL EVALUATION OF BIOMECHANICALLY INSPIRED HAND AND WRIST PROSTHESES

A Thesis

by

Mahsa Sarrafi Khosrowshah

Submitted to the
Graduate School of Sciences and Engineering
In Partial Fulfillment of the Requirements for
the Degree of

Master of Science

in the
Department of Mechanical Engineering

Özyeğin University
October 2023

DESIGN, DEVELOPMENT, AND FUNCTIONAL EVALUATION OF BIOMECHANICALLY INSPIRED HAND AND WRIST PROSTHESES

Approved by:

Assist. Prof. Ramazan Ünal, Advisor
Dept. of Mechanical Eng.
Özyeğin University

Assist. Prof. Özkan Bebek
Dept. of Mechanical Eng.
Özyeğin University

Assist. Prof. Elif Hocaoğlu
Dept. of Electrical and Electronics Eng.
Istanbul Medipol University

Date Approved: 10 August 2023

To my husband and family...

ABSTRACT

This thesis presents a comprehensive exploration and advancement in the field of hand and wrist joint prostheses designs. The primary objective is to address the limitations of current hand prostheses and enhance their functionality to provide improved support for upper-limb amputees in daily living activities.

The first aspect of this study focuses on the limitations of existing hand prostheses. Passive prostheses, although common, are hindered by their inability to perform a wide range of tasks, thus necessitating more advanced alternatives. Robotic prostheses offer precise motions and adequate force capabilities but face operational time and motor control challenges. To overcome these limitations, a novel design for a body-powered hand prosthesis is proposed. This innovative design is inspired by the natural movements of the human hand and incorporates a three-dimensional trajectory for the thumb. Elastic elements enable the prosthesis to return to its natural position after the application of forces through tendons from the opposite shoulder. With 8 degrees of freedom in the fingers, the prosthesis is prototyped using a 3D printer with ABS material. Performance evaluations demonstrate that this prosthesis, weighing 168 g, enables users to perform a wide range of activities of daily living, including pinching, grasping, and power gripping, thus significantly improving the functional capabilities of the hand prosthesis.

The second aspect of this research focuses on the importance of a wrist joint for upper-limb amputees. A new, lightweight, and stiffness pre-conditioned 2-DOF wrist joint is introduced specifically for transradial amputees. This wrist joint incorporates an innovative load-transferring mechanism, allowing modulation of joint stiffness to handle objects of varying weights. The use of a 3D printer with ABS material and a brushless DC motor for joint stiffness modulation results in a functional and practical wrist joint design. The successful functional evaluation

of the RoboWrist under different load settings proves its efficacy in adapting to the diverse weight requirements of handled objects.

By unifying these two aspects—novel hand prosthesis design and innovative wrist joint development, it is aimed to advance the field of prosthetics and significantly improve the quality of life for upper-limb amputees.

ÖZETÇE

Bu tez, el ve bilek eklemi protezleri tasarımlarının alanında kapsamlı bir araştırmayı ve ilerlemeyi sunmaktadır. Temel amaç, mevcut el protezlerinin sınırlamalarını ele almak ve üst ekstremite ampute bireylere günlük yaşam aktivitelerinde daha iyi destek sağlamak için işlevselliğini artırmaktır.

Bu çalışmanın ilk bölümü, mevcut el protezlerinin sınırlamalarına odaklanmaktadır. Pasif protezler yaygın olsa da, sınırlı sayıda görevi gerçekleştirememeleri nedeniyle daha gelişmiş seçenekler gerekmektedir. Robotik protezler, hassas hareketler ve yeterli kuvvet kabiliyetine sahip olsalar da, işletme süresi ve motor kontrolü zorluklarıyla karşı karşıyadır. Bu sınırlamaları aşmak için, vücut destekli bir el protezi için yeni bir tasarım önerilmektedir. Bu yenilikçi tasarım, insan elinin doğal hareketlerinden esinlenerek başparmak için üç boyutlu bir hareket içermektedir. Elastik elemanlar, protezin karşı omuzdan uygulanan kuvvetleri çıkardıktan sonra doğal pozisyonuna dönmesine olanak tanır. Parmaklarda sekiz serbestlik derecesine sahip olan protez, ABS malzemesi kullanılarak 3B yazıcı ile prototip haline getirilir. Performans değerlendirmeleri, 168 gram ağırlığındaki bu protezin, sıkma, kavrama ve güçlü kavrama gibi çeşitli günlük yaşam aktivitelerini gerçekleştirebileceğini gösterir, böylece el protezinin işlevselliğini önemli ölçüde artırır.

Araştırmanın ikinci bölümü, üst ekstremite ampute bireyler için bilek eklemi öneminde odaklanır. Bu çalışmada, özellikle transradial ampute bireyler için yeni, hafif ve ayarlanabilir 2 serbestlik dereceli önceden ayarlanabilir(Fleksiyon/ Ekstansiyon ve Radial/Ulnar deviasyon) bir bilek eklemi sunulmaktadır. Bu bilek eklemi, farklı ağırlıklı nesneleri işleme kabiliyeti için eklem sertliğini modüle etmek için yenilikçi bir yük transfer mekanizması içermektedir. ABS malzemesi kullanılarak 3B yazıcı ile prototip yapılan RoboWrist'in, eklem sertliğini farklı yük ayarları altında başarılı bir şekilde değiştirebildiği, böylece işlenen nesnelerin

farklı ağırlık gereksinimlerine uyum sağlayabildiği kanıtlanmıştır.

Bu tezde, yeni el protezi tasarımı, yenilikçi bilek eklem gelişimi ve üst ekstremite ampute bireylerin yaşam kalitesini önemli ölçüde artırmayı hedeflemekteyiz.

ACKNOWLEDGEMENTS

I extend my heartfelt gratitude to my thesis advisor, Asst. Professor Dr. Ramazan Ünal, for not only providing me with invaluable access to resources but also for his unwavering guidance during my M.Sc. journey. I would also like to express my sincere appreciation to Asst. Professor Dr. Barkan Ugurlu, Asst. Professor Dr. Özkan Bebek, and Prof. Dr. Bülent Yılmaz for their invaluable support and mentorship.

My deepest thanks go to my loved one, Omid Arfaie Khosrowshahi, and my family, my unwavering pillar of support, who have encouraged me throughout my M.Sc. studies.

Lastly, I thank to my colleagues who helped me during this thesis: Ege Gediksiz, Bariş Baysal, Tuğçe Ersoy, Burak Özkaynak, and Mustafa Derman.

This work is supported by the Scientific and Technological Research Council of Turkey (TUBITAK) with project 19E120.

TABLE OF CONTENTS

DEDICATION . . . . **iii**

ABSTRACT . . . . **iv**

ÖZETÇE . . . . **vi**

ACKNOWLEDGEMENTS . . . . **viii**

LIST OF TABLES . . . . **xi**

LIST OF FIGURES . . . . **xii**

I INTRODUCTION **1**

1.1 Literature review of hand prostheses 2

1.2 Literature review of wrist prosthesis 6

1.3 Outline of the thesis 7

II HANDMECH- DESIGN, DEVELOPMENT AND FUNCTIONAL EVALUATION OF A BODY-POWERED HAND PROSTHESIS **9**

2.1 Design of HandMECH 10

2.1.1 Thumb Design 10

2.1.2 Finger design 16

2.1.3 Returning the fingers to their home position 17

2.2 Prototyping 18

2.3 Experimental Evaluation 19

2.3.1 Multi-size object handling evaluation 20

2.3.2 Speed and durability performance evaluation 21

2.3.3 Functional Evaluation 22

2.3.4 Discussion 24

III ROBOWRIST: 2-DOF VARIABLE STIFFNESS ROBOTIC WRIST PROSTHESIS **27**

3.1 Method 27

3.1.1 Conceptual Design and CAD modeling 27

3.1.2 Structural Analyses 31

3.1.3 Tendons selection 33

3.1.4 Motor Selection 34
3.1.5 Simulation of the wrist stiffness 35
3.2 Prototyping 36
3.3 Experimental evaluation of RoboWrist 37
3.3.1 Wrist Prosthesis characterization 37
3.3.2 Functional evaluation 42
3.4 Discussion 47
IV CONCLUSIONS 50
REFERENCES 52
VITA 57

LIST OF TABLES

1 finger phalanges dimensions . . . 11
2 Fingers origin location in the local coordinates . . . 11
3 fingertips' configuration for 2P posture . . . 13
4 fingertips' configuration for 3P posture . . . 13
5 fingertips' configuration for 5P posture . . . 14
6 fingertips' configuration for 5G posture . . . 14
7 coefficients of fitted curve . . . 16
8 SAHP test results . . . 23
9 Performing daily activities with body-powered hand prosthesis . . . 24
10 Bills of the material of the wrist joint . . . 31
11 The properties of different wrist stiffness settings . . . 38

LIST OF FIGURES

1 The coordinate systems of the hand 11

2 Robotic schematic of fingers 12

3 The scatter plot of the calculated points for the thumb trajectory (a), the 3D fitted curve in MATLAB (b), realization of the trajectory in the CATIA (c) 16

4 Elongation of tendons in one finger joint: schematic of the tendon elongation (Left), The fully closed posture of the index finger (Right) 18

5 Prototype of the hand prosthesis: the fully open posture (Left), and the natural posture (Right) 19

6 The manufactured apparatus for the body-ablied to use the HandMECH during the experiments (a), the assembled HandMECH and the apparatus (b), an able-bodied subject wearing the HandMECH using the harness (c) 20

7 Multi-size object handling with HandMech: paper-cup(left), pen (middle), and card (right) 21

8 An able-bodied subject performs the BBT 21

9 SHAP test for body-powered hand prosthesis: top view (a), side view (b) 22

10 The CAD model of the rotating part (a), the CAD model of the base part(b), Ulnar deviation of the rotating part on the base part (c), Flexion movement of the rotating part on the base part (d) . . 29

11 Assembly of pulleys inside the wrist base part 30

12 The CAD model of the apparatus 30

13 Exploded view of the wrist joint 31

14 The total deflection (left) and Von-Mises stress (right) results for the R/U deviation in the wrist joint using ANSYS 32

15 The total deflection (left) and Von-Mises stress (right) results for the F/E movement in the wrist joint using ANSYS 33

16 The schematic of the wrist joint deviation when applying load . . . 35

17 torque-angle relation of the proposed wrist joint 36

18 2-DoF wrist prosthesis prototype 37

19 Experimental characterization of the wrist joint for F/E movement (Top): compliant (Left), stiff (Right) and Experimental characterization of the wrist joint for R/U deviation (bottom): compliant (Left), stiff (Right) 39

20 Experimental characterization results of the wrist joint for F/E motion . . . 40

21 Experimental characterization results of the wrist joint for R/U deviation . . . 41

22 Block diagram of the control system . . . 42

23 The wrist prosthesis position control when there is no load on the hand prosthesis . . . 43

24 The wrist prosthesis position control when there is 1kg load on the hand prosthesis . . . 43

25 The experiment environment of functional tests for wrist prosthesis 44

26 The delay of the motor's current response to the input signal when the filter is set 4000 μs . . . 45

27 The delay of the motor's current response to the input signal when the filter is set 140 μs . . . 46

28 The input and output signal of the motor . . . 46

List of Abbreviations

ADL Activities of Daily Living

F/E Flexion/Extension

R/U Radial/Ulnar

Abd/Add Adduction/Abduction

COM Center of Mass

DoF Degree of Freedom

FEM Finite Element Method

CAD Computer-Aided Design

DOB Disturbance Observer

PID Proportional-Integral-Derivative

RoM Range of Motion

CMC Carpometacarpa

MCP Metacarpophalange

PIP Proximal Interphalangea

DIP Distal Interphalangea

IP Interphalangeal

DC Direct Current

BBT Box and Blocks Test

SHAP Southampton Hand Assessment Procedure

CHAPTER I

INTRODUCTION

It is stated that in 2017, the global population grappling with limb amputation resulting from traumatic factors amounted to an estimated 57.7 million individuals [1]. The population of amputees in the United States is expected to be doubled by 2050 [2]. More than 12% of these amputees are transradial, including wrist joint and hand amputation [2]. Among the challenges faced by these individuals, the most prominent one lies in the successful integration of an artificial device to replace the lost limb, ensuring optimal rehabilitation outcomes [3]. Extensive research efforts are dedicated to developing and designing hand prostheses that aim to assist individuals in performing various activities of daily living (ADL) which can be classified according to the level of amputation and functionality of the prosthesis [3]. In designing hand and wrist prostheses for amputees, it is essential to consider the anatomical structure of these units to provide an anthropomorphic device. When considering the complexity of the human hand, it is noteworthy that it is composed of 27 bones and 28 muscles [4]. These intricate anatomical structures enable the hand to perform various functions, from delicate manipulations to forceful grips. Understanding the intricate interplay between these bones and muscles is crucial in designing prosthetic devices that closely mimic the capabilities of the natural hand. While anthropomorphic and dexterous hand prostheses are developed and show high capabilities in performing various tasks, including ADL, the importance of having a well-designed wrist prosthesis cannot be overlooked. A proper wrist prosthesis plays a vital role in improving the overall functionality of hand prostheses, allowing users to perform a wider range of tasks with greater ease and efficiency. In the last two decades, the rejection rate for intrinsically powered hand prostheses lacking wrist joints is consistently exceeded

20% [5, 6, 7, 8], with more than 50% amputees experiencing significant pain and injury to their remaining and intact limbs, as well as other areas of the body, such as the trunk, neck, and back [9, 10, 11]. Sardelli et al. investigate whether myoelectric prosthetic hand users can achieve enhanced performance with the presence of a passively flexible or manually adjustable prosthetic wrist compared to having no wrist functionality [12]. This study indicates that using a wrist prosthesis in combination with a hand prosthesis would improve ADL's efficiency. A study by Montagnani et al. proposes the hypothesis that a single DOF hand prosthesis with a wrist F/E prosthesis can achieve similar functionality as a multi-DoF hand without wrist prosthesis [13]. The impact of using a wrist prosthesis with a hand prosthesis shows the value of prosthetic wrists, which can enhance dexterity while reducing reliance on intact limbs and compensatory movements. This prosthesis can enhance user ability in ADL and reduce the risk of joint injuries. Several studies show that full wrist mobility may not be necessary for individuals to perform daily activities, based on observations made during the performance of these activities [12, 14, 15].

1.1 Literature review of hand prostheses

Aesthetic and powered prostheses (body-powered and electrically powered) are the most conventional solutions for amputations [16]. The main goal of cosmetic gloves is to cover the mechanism of the hand prosthesis and prevent any damage to these mechanisms [17]. Additionally, without a hand prosthesis, these types of gloves only try to mimic the anthropomorphic of the human hand, and they are incapable of performing most of the ADL. Although body-powered hand prostheses can realize most of the ADL, providing adequate force to the fingers and controlling the movements of the prosthesis are still challenges of the hand prosthesis design. Thus, active prostheses are addressed to solve such problems. Krausz, et al. [18] research is focused on developing active hand prostheses to achieve desired force values and precise finger movements. They design a 6-DOF hand prosthesis for testing control algorithms. For testing purposes, a Sinometer HY3020E DC power supply and a 10 lb load cell from Load Cell Central are used to measure torques and forces. The first test involves measuring the motor torque with and without the gearhead. Using a known beam length and the load cell, they calculated the motor torque produced, recorded as 1.6 N-m with a 246:1 gearhead and 6.4V applied voltage. The next test involves the assembled finger and hand. The finger is extended, and the force sensor measures the force at the fingertip. With the same gearhead, the fingertip force is measured as 4.12 N with a voltage of 6.4V. The finger take approximately 0.7 s to curl to a 90° position, indicating a finger closing speed of 2.24 rad/s. However, the actual fingertip forces are lower than theoretical values due to optimistic motor specifications and losses in the transmission system. Several studies try to transfer the DC motor motion to the joint of the fingers using linkage mechanisms. Li et al. [19] propose a novel finger structure for a robotic hand. The design combines a linkage mechanism and springs to achieve coupled, self-adaptive motion. They also introduced a transmission mechanism to connect the independent fingers, enabling cooperative movement without the need for additional actuators. This results in enhanced self-adaptability for the entire hand. Additionally, a method to calculate contact forces for achieving grasping stability is introduced, ensuring the hand can adjust to irregularly shaped objects without complex control strategies and sensors. This innovation allows the hand to attain a grasping static equilibrium range. Peerdeman et al. [20] present a design with a four-bar linkage to actuate four fingers with a single DC motor. This hand has a joint locking mechanism to control hand-grasping motions. Additionally, this joint lock allowed the prosthesis to actively control the DOF of the fingers by a single DC motor. In order to demonstrate the effectiveness of the joint locking mechanisms, a 250 g weight is suspended from the tip of the index finger. Without the engaged joint locks, the finger flexed upon releasing the weight. However, when the joint locks are activated, the finger remained straight, even if the solenoid actuators are subsequently disabled. Bennett et al. [21] present a hand configuration and conduct experiments to assess hand performance, specifically focusing on digit force capabilities through an embedded system design. The electrical power requirements for grasping and releasing an object are evaluated using a 500 mL water bottle filled with a mass of 500 g. The grasping action is repeated ten times, with an average current requirement of 2.25 A·s and an average energy requirement of 31.5 J, comparable to the energy needed for the posture sequence. The tested hand prototype utilizes a 14 V, 1.35 A·h lithium polymer battery weighing 133 g, providing a gravimetric energy density of 511 J/g. With this battery, the hand can perform approximately 2100 power grasps or execute around 2300 movement sequences on a single charge. Although the robotic hand prostheses provide precise motion and adequate power during the ADL, they require batteries or a power supply to actuate the motors. This brings extra weight and limits the active time of the hand prosthesis. Hence, developing a body-powered prosthesis that can perform most ADL would be more beneficial. Moreover, body-powered prostheses are cost-effective, reliable, and durable [22, 23]. Furthermore, putting the user in the loop would be more effective in user acceptance.

Herath et al. [24] develop a hand prosthesis featuring a linkage finger to enable appropriate finger movements for grasping cylindrical and spherical objects in a power grasp. The work envelope of a finger refers to its range of motion, which is limited to a specific area. To assess the capabilities of the proposed hand design, Solidworks motion simulations are further employed to examine its ability to perform both cylindrical and spherical grasps, as depicted. The prosthetic hand demonstrated the capability to grasp a cylinder with a diameter of 75mm and a sphere with a diameter of 85mm at maximum finger flexion. The maximum diameters of the cylinder and sphere that the hand can grasp are determined to be 100mm and 110mm, respectively. Unal and Toker[25] propose a voluntary opening (VO) and closing (VC) hand, which is able to provide a prosthetic hand with low mass and is easy to use for amputees. James et al.[26] demonstrated a terminal device capable of VO and VC modes, meeting the requirements for ADL and allowing users to switch between modes. The Southampton Hand Assessment Procedure (SHAP) is followed, including task practice before the timed test to reduce bias and improve familiarity with each prehensor. Subjects utilized VO/VC prehensor to perform 26 tasks representing various grasps and daily activities. Recorded task times are normalized and entered into the SHAP website, which calculated an index of functionality (IOF) [26]. Brokaw et al. [27] develop a passive hand prosthesis utilizing elastic cords to assist hand opening by applying an extension torque to the finger joints. A force-torque sensor is used to measure torque at a known distance from the finger component's center of rotation. Torque profiles are adjusted to match each subject's tone profile, with three settings tested for the first version and three different settings tested for the second version of the device. Functional testing involved moving the hand from a start position to lift and place blocks of varying widths. The device is used both with and without the subject's unaffected limb for assistance [27]. Jung et al. [28] propose a tendon-driven hand prosthesis with five fingers and six DOF capable of performing ADL tasks and hand postures. The flexion motion is driven by a geared DC motor with a gear ratio of 1:64, and the motor provides two phase-encoder signals. An RC-servo motor with an adjustable rotation angle based on a command pulse duty ratio controls the thumb's rotation motion. Some researchers, such as Smit et al. [29], try to decrease the mass of the body-powered prosthesis. They obtain the Delft Cylinder Hand, with a mass of 55%–68% lower than that of the lightest current prosthetic hands. Therefore, designing a lightweight body-powered hand prosthesis with the highest capabilities to perform the ADL would be the main goal of the hand prostheses. Cobos et al. [30] investigate the kinematics of the human hand during manipulation tasks using a 24-DOF model. To simplify the model, they exclude certain less significant DOF and create two reduced versions with 6 and 9 DOF, respectively. These reduced models focus on the main independent joints of the thumb, index finger, and little finger while considering the middle and ring fingers as coupled with the index and little fingers. Finding the optimal number of DOFs for accurately describing hand postures is important, and this involves balancing the acceptable level of error with the minimum number of DOF required for the intended application.

To realize the biomechanics of the human hand, the biomechanical data of hand movements in ADL is essential. Shimawaki et al. [31] present a study in motion analysis of flexion angles of the finger joint in the ADL using X-Ray technology. Lee, Kyung-Sun, et al. [32], using a VICON system, identify finger joint angles in different hand movements during daily activities for cylindrical and square shape objects. Despite performing most of the ADL, the current hand prostheses still face many challenges like complexity, weight, operation, and response time.

1.2 Literature review of wrist prosthesis

The human wrist has 3 degrees of freedom (DOF) that enable movement in flexion/extension (F/E), radial/ulnar (R/U) deviation, and pronation/supination (P/S) [33]. Each of these movements has a defined range of motion (ROM), such as a F/E range of $-73°$ to $76°$ and a R/U deviation range of $-25°$ to $45°$ [34, 35]. The functional ROM, which reflects the usefulness of each DOF for performing ADL, is significantly lower than the maximum ROM in both F/E and P/S. The functional ROM for F/E and R/U is $-54°/48°$ and $-22°/38°$, respectively [36, 37, 38].

Designing and evaluating transradial prostheses are studied as research projects and commercial products. Most of them focus on hand prostheses and their ability in activities of daily living (ADL). Wrist prostheses can be classified based on the type of actuation they use into three categories: passive, body-powered, and active joints. Passively actuated wrists rely on external forces and torques to reorient the end effector and are often used to achieve the opening and closing of a terminal device [39]. Passive devices may also use friction clutches or locking mechanisms in their components to prevent wrist motion after positioning. These mechanisms can lock movement after a specific angle using a pin or button [40, 41]. Body-powered wrist prostheses use a body harness and bowden cable, allowing the amputee to exert forces and torques from the opposite or same shoulder to orient the wrist position. These prostheses may incorporate a single rotational joint or a 2-DOF joint [42, 43]. Passive and body-powered wrist prostheses may not be able to provide sufficient forces and precision, leading to the development of active prostheses that use electrical actuators to generate motion in the end-effectors. For example, Peter et al. propose a 2-DOF prosthetic wrist with two DC motors to enable P/S and F/E movements [44]. In addition to precision, controlling wrist stiffness in F/E and R/U movements is important for designing wrist prostheses that can hold the prosthetic hand and the grasped object in a fixed position. There are a few studies that have examined the variable stiffness of the wrist joint. For instance, Federico et al. use a 2-DOF differential mechanism that allows the wrist prosthesis to have switchable stiffness [45]. Regarding adjusting the wrist joint stiffness, some research focus on developing frameworks to estimate human hand-wrist joint stiffness, such as the work by Domenico Formica et al., who uses a setup without a robot hand [46]. As a result, the challenge of developing a compact and lightweight variable stiffness wrist joint prosthesis remains an important area of research in the field of upper limb prosthetics.

1.3 Outline of the thesis

This thesis is organized as follows. In Chapter I, the importance of hand and wrist prostheses for amputees is illustrated. Additionally, in this chapter, the literature review of these prostheses and the challenges in the current prostheses are illustrated.

In Chapter II, the design, development, and evaluation of a biomechanically inspired hand prosthesis is presented. The proposed body-powered prosthesis, having a 3D trajectory for the thumb and an anthropomorphic design of the hand prosthesis, tries to mimic human hand behavior.

Chapter III illustrates the design, development, and evaluation of a 2-DOF stiffness variable wrist prosthesis that can adopt the joint stiffness according to the object weight handled by the hand prosthesis. The characterization and functional evaluations of this prosthesis are presented in this chapter.

In Chapter IV, the conclusion of the study is presented. Additionally, future works are proposed in this chapter.

CHAPTER II

HANDMECH- DESIGN, DEVELOPMENT AND FUNCTIONAL EVALUATION OF A BODY-POWERED HAND PROSTHESIS

The current hand prostheses are designed to provide the daily living activities of amputees. According to the type of actuation, the hand prosthesis can be classified as passive (opening or closing using a terminal device), body-powered (opening or closing using the opposite shoulder and harness), or active prostheses. Passive prostheses have many limitations, and most of them can perform only a limited number of tasks. Although robotic prostheses provide precise motions and adequate forces to perform the tasks, their operation time and motor controlling challenges are still the limitations of these actuators. This study proposes a novel design for a body-powered hand prosthesis. With inspiration from the human hand, a three-dimensional (3D) trajectory for the thumb is designed, replicating the path of the thumb's movements during different tasks. Additionally, using elastic elements, the prosthesis can return to its natural position after removing the forces applied by the opposite shoulder through the tendons. The proposed prosthesis has 8 degrees of freedom in the fingers and is prototyped within a 3D printer using ABS material. The performance evaluations, including the Southampton Hand Assessment Procedure (SHAP), Box and Blocks test (BBT), and a person's daily activities, show that this prosthesis with a 168gr mass can perform many activities of daily living (ADL), such as pinching, grasping, and power griping. The proposed body-power prosthesis in this chapter is named HandMECH, and it is able to perform a similar test of SHAP test in 29 sec and pick and place 16 blocks in one minute during the BBT. The proposed hand prosthesis is capable of holding the object from 1-120 mm thickness.

2.1 Design of HandMECH

A body-powered hand prosthesis is designed to perform the human hand's main tasks, such as pinching and grasping. Since the middle, ring, and little fingers' functions during the ADL are similar to each other, a triple finger is considered instead of these three fingers. While the triple and index fingers include three joints (metacarpophalangeal (MCP), proximal interphalangeal (PIP), distal interphalangeal (DIP)), the thumb finger includes only two joints (MCP, Interphalangeal (IP)). The base of the thumb moves on a 3D trajectory which resembles the Flexion/Extension (F/E) and Abduction/Adduction (Abd/Add) movements of the carpometacarpal (CMC) joint of the thumb. The following sections of the HandMECH design illustrate the thumb design, 3-finger design, and energy recycling mechanism design.

2.1.1 Thumb Design

There are 5 DoF in the thumb, three of which are located in the CMC joint [47]. The most dominant DoFs in the CMC joint are F/E and Abd/add movements allowing rotational movements in different axes. Combining these two rotations allows us to consider a prismatic joint path in the MCP joint of the thumb. The forward kinematics is employed to determine the thumb's fingertip positions. A Newtonian reference frame is established at the hand's lower right corner, and each finger's coordinate system origins are assumed to be at the middle base of the MCP joints. These coordinate systems' origin locations are measured according to the hand of one of the authors in this study and are listed in Table 1. In Table 2, the distances between the local origins and the origin of the thumb are listed. Fig. 1 illustrates the coordinate system and the positions of the finger origins on the hand.

Table 1: finger phalanges dimensions

Phalange	Index (mm)	Middle (mm)	Ring (mm)	Little (mm)
Proximal phalange	44	49	46	37
Middle phalange	26	31	29	20
Distal Phalange	26	27	26	22

Table 2: Fingers origin location in the local coordinates

Coordinate	Index (mm)	Middle (mm)	Ring (mm)	Little (mm)
X	-16	-34	-46	-63
Y	26	29	26	22
Z	0	0	0	0

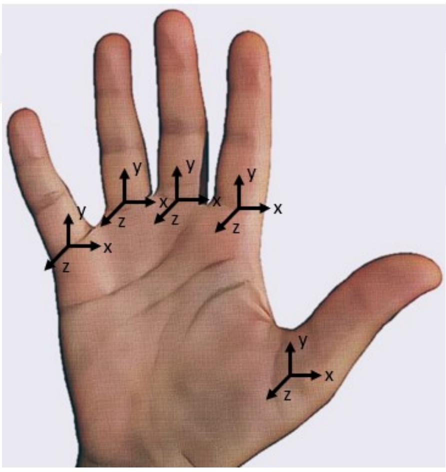

Figure 1: The coordinate systems of the hand

By utilizing joint angle information for ADL obtained from previous studies [31, 32], it is possible to determine the fingertip location through forward kinematics based on the established coordinate system. In order to classify the fingers' orientation during various ADL (classifying as pinching, lateral pinching, and grasping), five major orientations for the fingers are assumed based on [32], which are denoted as 2P, 3P, 4P, 5P, and 5G. The "P" stands for pinching, and the "G" stands for grasping, while the numerical value indicates the number of fingers involved in the respective activity, including the thumb. For instance, 3P signifies the pinching activity performed by the thumb, index finger, and middle finger. Using this terminology for different orientations of the hand fingers, various ADL such as pinching and grasping, are clearly identifiable. By employing forward kinematics and taking into account the coordinate system and defined origins, the locations of the fingertips can be computed. Given that only F/E is considered for joint rotation, rotations around the X-axis are considered, as depicted in Fig. 2.

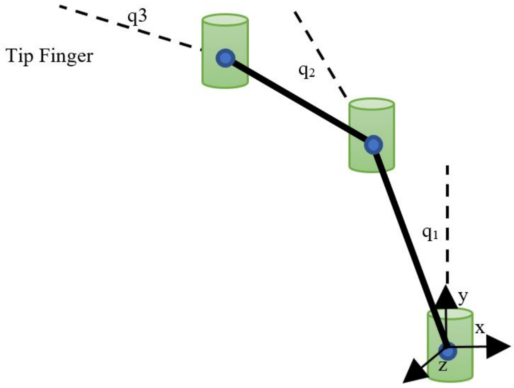

Figure 2: Robotic schematic of fingers

Fig. 2 shows the robotic schematic of a finger, including three joints (MCP, PIP, and DIP joints) and the flexion angles of each joint. In this figure, q_1, q_2, and q_3 are the MCP, PIP, and DIP joints' F/E angles, respectively. Additionally, l_1, l_2, and l_3 represent the length of the Proximal, Middle, and Distal Phalanges, respectively. The fingertip position would be determined according to the forward kinematics of a 3DoF planner robot rotating around the X-axis. According to this, the fingertips position are as follows,

$$P_y = l_1 \cos q_1 + l_2 \cos(q_1 + q_2) + l_3 \cos(q_1 + q_2 + q_3) \quad (1)$$

$$P_z = l_1 \sin q_1 + l_2 \sin (q_1 + q_2) + l_3 \sin(q_1 + q_2 + q_3) \quad (2)$$

In Eqs.1 and 2, P_y and P_z indicate the location of the fingertips. Since the rotation is around the X axis, only the position of fingertips in the Y and Z axes is calculated. According to Eq.1 and 2, the fingertips of all fingers regarding the specified posture of the hand are determined. The locations of each fingertip and the rotation angles for each mode are provided in Table 3-6.

Table 3: fingertips' configuration for 2P posture

2P joints rotation (deg)	
Joint	Index
MCP	51.86
PIP	27.6
DIP	22
Fingertips global coordination (mm)	
X	-16
Y	32.85
Z	68.76

Table 4: fingertips' configuration for 3P posture

3P joints rotation (deg)		
Joint	Index	Middle
MCP	43.1	48.2
PIP	31.4	46
DIP	24.1	10.9
Fingertips global coordination (mm)		
X	-16	-34
Y	41.19	32.36
Z	81.83	94.51

Table 5: fingertips' configuration for 5P posture

5P joints rotation (deg)				
Joint	Index	Middle	Ring	Little
MCP	34.7	40.3	41.9	0
PIP	35.6	50.5	46.9	20.1
DIP	23.9	17.7	11.8	21.6
Fingertips global coordination (mm)				
X	-16	-34	-46	-63
Y	49.03	37.37	36.06	74.21
Z	76.46	89.29	86.27	22.51

Table 6: fingertips' configuration for 5G posture

5G joints rotation (deg)				
Joint	Index	Middle	Ring	Little
MCP	40.8	53	60.6	0
PIP	56.2	59.9	60.3	38.9
DIP	37.4	35.9	30.1	51.2
Fingertips global coordination (mm)				
X	-7	-24.14	-42.19	-63.21
Y	69.13	64.14	52.71	97.35
Z	59.51	68.96	66.44	27.32

To ensure comprehensive coverage of the thumb trajectory, it is assumed that the thumb maintains contact with all fingertips. Thus, the thumb fingertip can be considered equivalent to the fingertips of the other fingers in all movements. In the simplest approach to determine joint locations, rotation around the X-axis is assumed for the thumb, similar to the other fingers. Following this, thumb angles are determined with the inverse kinematics. The following equations are utilized to determine these joint angles.

$$cosq_2 = \frac{\left(\frac{P_y - y_0}{cosq_0}\right)^2 + (P_z - z_0)^2 - {l_1}^2 - {l_2}^2}{2l_1l_2} \tag{3}$$

$$cosq_1 = \frac{B.\frac{P_y - y}{cosq_0} + A(P_z - z)}{A^2 + B^2} \tag{4}$$

$$A = l_1 + l_2.cosq_2, B = l_2.sinq_2 \tag{5}$$

$$\frac{sinq_0}{cosq_0} = -\frac{P_x - x}{P_y - y} \tag{6}$$

In Eqs.3-6, l_1 and l_2 are the dimension of the thumb Proximal Phalanx (PP) and Distal Phalanx (DP) links, respectively, and q_0, q_1, and q_2 are the Abd/Add angle of the CMC and F/E angle of the MCP and PI joints of the thumb. Additionally, in these equations, x_0, y_0, and z_0 are the coordinates of the thumb base location, and because this location is assumed to be the origin of the coordinate systems, they are considered as zero. The Cosine law is used to determine the q_2 joint angles, and it is used to determine the q_1 through the Eqs.4-6. Finally, the Abd/Add angle of the thumb can be determined with Eq.6. Unique Abd/Add angles are calculated for each specific posture of the hand and each of the fingers. The joint angles of the thumb finger would be implemented to determine the thumb base trajectory. With known thumb joint angles, forward kinematics starting from the calculated tip fingers can determine the thumb base position as shown in the scatter plot in Fig.3-a.

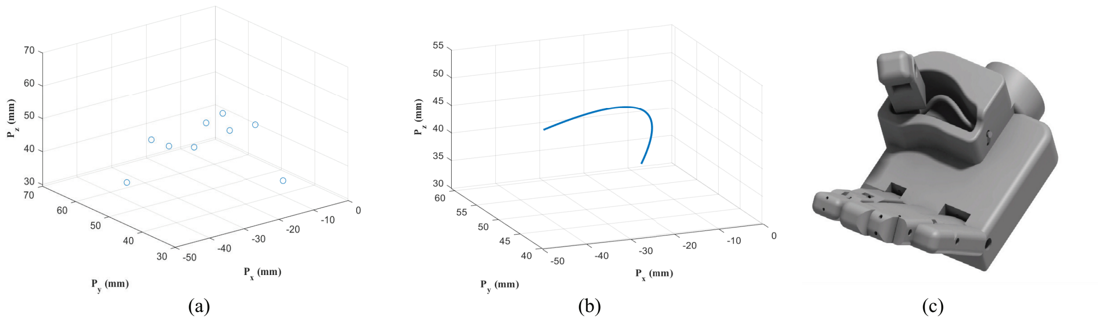

Figure 3: The scatter plot of the calculated points for the thumb trajectory (a), the 3D fitted curve in MATLAB (b), realization of the trajectory in the CATIA (c)

In Fig.3-a, the coordinates of the base of the thumb for each defined task (2P, 3P, 5P, and 5G) are shown as points. After calculating these points in MATLAB, a 3D curve is fitted to these data as shown in 3-b. The obtained coefficients for the polynomial curve are presented in Eq.7.

$$
\begin{aligned}
y &= p_{0y} + p_{1y}x + p_{2y}x^2 \\
z &= p_{0z} + p_{1z}x + p_{2z}x^2
\end{aligned}
\tag{7}
$$

Where the p_{iy} p_{iz} are the coefficient of the curve equation and are defined as follows:

Table 7: coefficients of fitted curve

p_{0y}	p_{1y}	p_{2y}	p_{0z}	p_{1z}	p_{2z}
73.1	1.96	0.03	16.5	-2.33	-0.03

The palm dimension is inspired by the anatomical structure of the human hand and is split into upper and lower parts to facilitate printing and accommodate additional mechanisms. The 3D trajectory is realized by implementing the calculated points in the CATIA environment, as shown in Fig.3-c.

2.1.2 Finger design

In the design of the HandMECH prosthesis, three fingers are considered, and the thumb design is illustrated in the previous section. The index finger includes three joints (MCP, PIP, and DIP), which are assumed to perform only F/E movements. Furthermore, in order to reduce the number of DoFs and due to the analogous functions of the middle, ring, and little fingers during ADL, these three fingers are regarded as a collective unit referred to as the triple finger. Similar to the index finger's three revolute joints, MCP, PIP, and DIP joints are considered in the triple finger. The dimensions of each finger segment are determined based on measurements taken by one of the authors of this study, which are listed in Table1.

2.1.3 Returning the fingers to their home position

Based on the characterization provided in Berning et al.'s study [48], the HandMECH prosthesis is identified as a versatile prosthesis encompassing both VC prosthesis functionality, utilizing finger tendons in conjunction with force application from the opposite shoulder for grasping objects and restoring fingers to their original positions post-task completion, and VO prosthesis functionality, achieved by incorporating supplementary tendons at the shoulder and employing springs to retract the tendons via the shoulder. For the purpose of this study, the focus is solely on the VC aspect of the HandMECH to prevent the complexity of the prosthesis. The study incorporates the use of three springs. Each spring returns the thumb, index, and triple finger to their initial positions without requiring additional energy. The fingers are connected to the springs through tendons. The flexion of the tendons at each joint is calculated to design the springs of the prosthesis and determine the required stiffness. During finger joints' flexion, the springs extend, and the deflection of each spring can be calculated based on the flexion angle at each joint. Considering that the tendons pass through the joints of the fingers, friction forces at each joint are also considered in the calculations. As the tendons pass through approximately one-third of the fingers' thickness, the elongation at each joint can be determined using the cosine law, as illustrated in Fig.4.

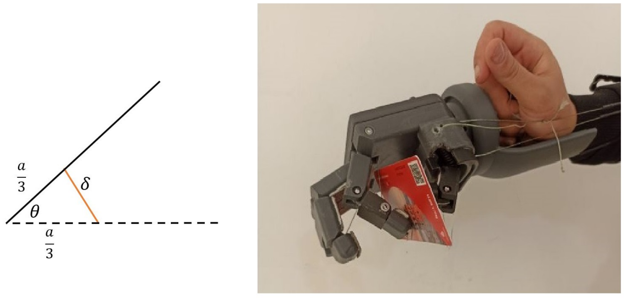

Figure 4: Elongation of tendons in one finger joint: schematic of the tendon elongation (Left), The fully closed posture of the index finger (Right)

In Fig. 4 (left), the natural and flexed postures of the finger width are shown with dashed and solid lines. The index fingers' position in the pinching and the schematic of the tendon elongation are shown. a is the width of the finger, and θ is the flexion angle of each joint. Therefore, the overall deflection of the spring can be calculated as Eq. 8:

$$\delta = \frac{a}{3}\left(\sqrt{2\left(\cos\theta - 1\right)}\right) \tag{8}$$

All phalanges are assumed to have equal thickness in this study. The deflection of the tendon at the MCP, PIP, and DIP joints is denoted as δ_{MCP}, δ_{PIP}, and δ_{DIP}, respectively. Considering the parameters' magnitudes in Eq.8 and the maximum flexion angles observed during daily activities, the total elongation in the index and triple fingers is calculated as 11.64 mm and 12.95 mm, respectively. The applied loads on the spring are calculated according to the required force to return the finger phalanges from the flexed position to their natural position. Considering the design limitations, the selected springs for the index and triple fingers have an outer diameter of 8 mm and a wire diameter of 0.75 mm. A stiffness of $0.3\frac{N}{mm}$ satisfies the dimension limitations and also the deflection requirement.

2.2 Prototyping

The HandMECH prosthesis is fabricated using an UltiMaker2^{+} 3D printer and ABS material. The printed components are assembled using 3mm pins, and the upper and lower sections of the palm are connected using M3 bolts. Springs were installed in the palm and along the thumb trajectory, with their bottoms securely fixed to the joints using glue (Evo Bond 502 Super Glue). Ball bearings (MR 63-ZZ) are used between the pins and the finger joints to allow a smooth and less friction rotation in the finger joints. The printed hand prosthesis in fully opened (right) and natural (left) postures are depicted in Fig.5.

Figure 5: Prototype of the hand prosthesis: the fully open posture (Left), and the natural posture (Right)

2.3 Experimental Evaluation

These evaluations are approved by the Clinical Research Ethics Committee of Erciyes University with document number 2019/32. These evaluations include multi-size object handling to evaluate the functionality of the HandMECH prosthesis, speed and durability performance to evaluate the HandMECH prosthesis's speed in holding and applying pinching force to replace blocks in the BBT, and functional evaluation of the prosthesis to pick and place experiment of the multi-shape object and measuring the performance time. To perform these experiments with an able-bodied subject, an apparatus must be connected to the HandMECH prosthesis and held by the subject. Fig.6 shows the manufactured apparatus for the body-ablied to use the HandMECH during the experiments (a), the assembled HandMECH and the apparatus (b), an able-bodied subject wearing the HandMECH using the harness (c).

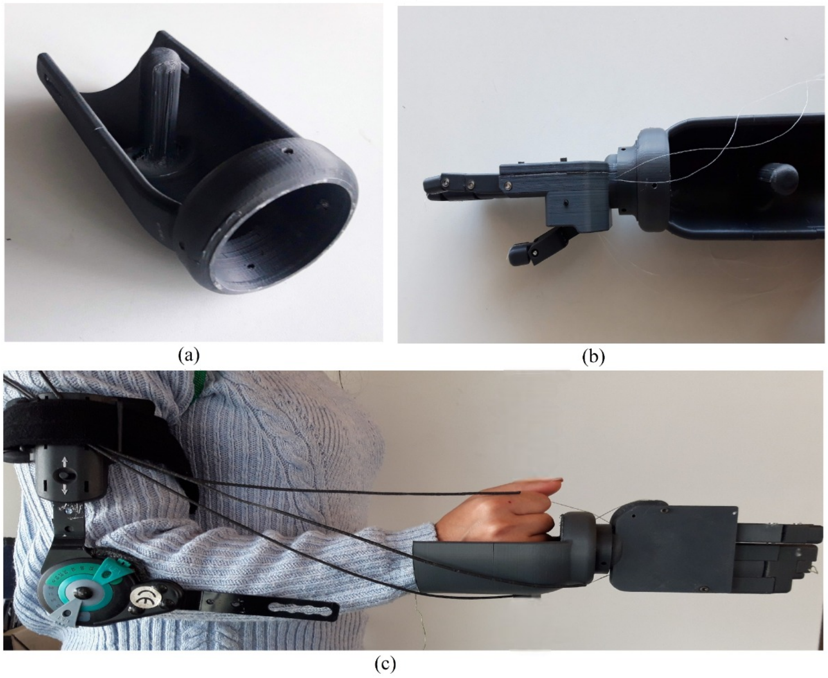

Figure 6: The manufactured apparatus for the body-ablied to use the HandMECH during the experiments (a), the assembled HandMECH and the apparatus (b), an able-bodied subject wearing the HandMECH using the harness (c)

2.3.1 Multi-size object handling evaluation

Since among the ADL, there are different multi-size objects to be held by the hand; the HandMECH must be able to hold all these objects with different sizes. Additionally, applying a controlled force to the objects is important to prevent damage. Therefore, in these experiments, different objects with different sizes are evaluated. The ability of the HandMech prosthesis to hold objects such as plastic glass with a diameter of 70mm, pencils with a diameter of 70mm, and debit rectangle cards with $54 \times 85 \times 1mm$ is investigated. This part aims to successfully hold and carry these objects for a distance of at least 20cm. While holding the empty plastic glass, the pinching forces are carefully controlled to prevent any damage or deformation to the glass. The corresponding images of these tests are presented in Fig.7.

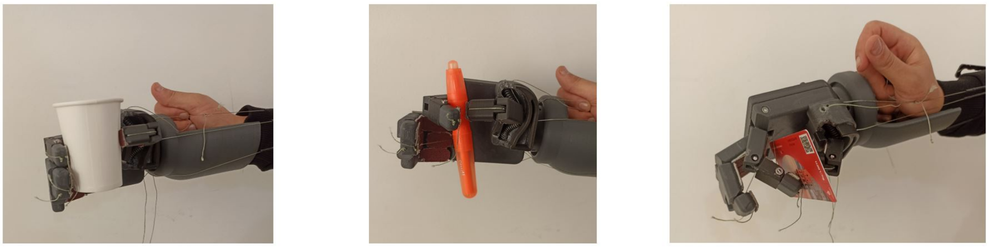

Figure 7: Multi-size object handling with HandMech: paper-cup(left), pen (middle), and card (right)

2.3.2 Speed and durability performance evaluation

A modified version of the BBT is conducted to assess the speed and durability of the hand prosthesis. This evaluation method is employed in many studies [29, 49, 50]. Following the methodology described in [50], a box divided by a plate is utilized. The box contains 26 rectangular wooden cuboid blocks with the dimension of $70 \times 27 \times 22mm$, which are initially positioned on one side of the box. The participant is asked to be accustomed to the procedure before commencing the test. Within a time limit of 60 seconds, they are required to pick up the blocks from one side of the box and transfer them to the empty side, crossing over the barrier. This task is repeated three times, with a 30-second rest period provided between each trial. The number of successful block transfers within the designated time frame is recorded. Fig. 8 illustrates the BBT performed with the HandMECh prosthesis. The test results indicated that the participant successfully moved 13, 14, and 16 blocks to the empty side within the 60 s.

Figure 8: An able-bodied subject performs the BBT

2.3.3 Functional Evaluation

A modified version of the SHAP test is employed to assess the functionality of HandMECH in various ADL with different shapes and masses. As described in [51], this evaluation method measured the user's ability to perform various grasping tasks, including spherical, power, tip, tripod, lateral, and extension grasping. Fig. 9 illustrates the six shapes utilized in this test: small and big cylindrical, spherical, small and big rectangular prism, and triangular prism. These shapes were selected to simulate real-world objects encountered during ADL.

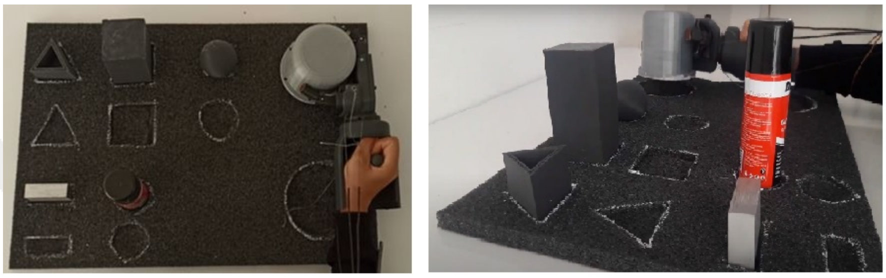
(a) (b)

Figure 9: SHAP test for body-powered hand prosthesis: top view (a), side view (b)

.

A variety of shapes are employed in the experimental tests, including two cylindrical shapes, a cylindrical water bottle, a conic glass, a mobile phone, a comb, a toothbrush, a key, and a triangular prism. The detailed specifications of these shapes are given in Table 8.

Table 8: SAHP test results

Shape	Dimension (mm)	Mass (g)	Task Duration (s)
Big Cylinder	94×100	178	3
Small Cylinder	40×120	267	3
Sphere	R=60	46	2
Triangle Prism	$60 \times 60 \times 45$	34	5
Rectangular Prism	$60 \times 60 \times 120$	120	4
Rectangular block	$20 \times 45 \times 60$	150	6

The total duration of performing all the tasks in the SHAP test is 39 s, including the duration of each task, the movements of hand prosthesis between the tasks, and any repeat of the tasks in case of failure to perform them. This period for picking and placing the objects in the predefined locations is 29 s, as indicated in Table 8. Partial illustrations of the evaluation are provided with a video attached to this manuscript. In addition to these tests, HandMECH prosthesis is evaluated in performing some of the common daily activities listed in Table 9.

Table 9: Performing daily activities with body-powered hand prosthesis

Daily activity	Picture	Daily activity	Picture
Tooth-brush	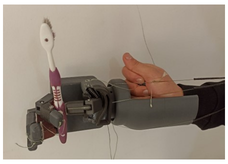	Hair comb	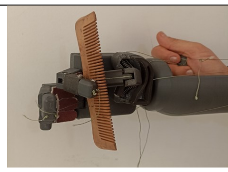
Key	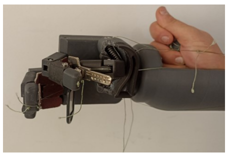	Water bottle	
Water pouring		Mobile phone	
Mouse		Mug	

The results of these experiments show that most of the ADL, such as the tasks including small and fragile objects and the tasks with heavy and big objects, can be performed using HandMECH.

2.3.4 Discussion

The HandMECH prosthesis has a total mass of 168 grams, making it significantly lighter than the mass of the existing hand prostheses on the market (347-600 gr)[29]. This reduced weight would lead the amputee to accept and utilize the prosthesis comfortably. Notably, the mass of the HandMECH is 10% lighter than Cyborg beast (184.2 grams), and it is 10% heavier than the Delf cylinder hand [52, 29]. Using hollow pins instead of steel ones in the joints of the HandMECH can reduce the mass of the prosthesis. Additionally, topology optimization of HandMECH based on the functions would reduce the mass of the prosthesis. Moreover, reducing the infill of the printing to an acceptable portion, according to the structural analysis, would decrease the mass of the prosthesis.

Regarding ease of use, the HandMECH incorporates a novel 3D trajectory for the thumb base, eliminating the need for two additional degrees of freedom (DoFs) in the hand design. This innovative 3D thumb trajectory enables the HandMECH to execute a wide range of daily activities, including lateral pinching, pinching, and grasping. Consequently, the prosthesis offers enhanced dexterity to hold objects from 1mm thickness to 120mm diameter. Furthermore, treating the middle, ring, and little fingers as a unified unit finger reduces the required DoFs and overall complexity of the prosthesis. This approach eliminates the necessity for additional components, such as bearings or springs, effectively decreasing the total mass of the prosthesis.

Functionality tests are conducted to evaluate the performance of HandMECH. The average number of blocks transferred during BBT is measured to be 14.3 with a maximum of 16 blocks, which demonstrates an 18% improvement compared to [51] in the case without adding extra friction. However, compared to other benchmark prostheses (which achieve 17-30 blocks) [49, 53], the HandMECH indicates slightly lower functionality. It is worth noting that the larger size of the blocks used in these experiments may have influenced the results, and standardization of the test protocol is expected to enhance functionality. The modified SHAP test results indicate that HandMECH is capable of performing most ADL, implying the improvement of the user's quality of life. The average trial time of the experiment shows that the HandMECH prosthesis performs 41% better than the F3HAND II [54]. Additionally, the overall task time is 22% less than the Mouchoux et al. study [55]. Furthermore, the prosthesis effectively handles tasks such as holding and carrying a full bottle of water, showcasing its strength and versatility despite being constructed from ABS material, while the other 3D-printed hand prosthesis is designed for only a certain level of functionality[51]. It must be noted that this study introduces a prototype of the HandMECH prosthesis, whereas other prostheses being compared are either commercial products or, in advanced stages of development, nearing commercialization [29].

During the experiments, it is observed that the HandMECH exhibited less friction in the fingers, resulting in a reduced ability to move blocks during the BBT. Additionally, the unique 3D trajectory followed by the thumb in the HandMECH design caused variations in the direction of the thumb tendon. This change in tendon direction affects the amount of force applied to objects held by the prosthesis. It is planned to reduce the mass of the HandMECH prosthesis further. Furthermore, 3D curve realization is done straightforwardly, and this would be refined with a more efficient sliding mechanism in terms of friction. Additionally, joint friction can be reduced by changing the geometry and tendon pathway. On the other hand, friction would be optimized for better gripping performance by using rubber in the fingers. In the current design, the positioning and rotation of the thumb with one pulley are controlled. In the next version it is aimed to extend this approach by controlling the thumb position via wrist rotation and comparing it with this one in terms of ease of use.

CHAPTER III

ROBOWRIST: 2-DOF VARIABLE STIFFNESS ROBOTIC WRIST PROSTHESIS

The need for a wrist joint together with a hand prosthesis is essential for upper-limb amputees. This study presents a new, lightweight, and adjustable 2-DoF (Flexion/Extention (F/E) and Radial/Ulnar (R/U) deviation) wrist joint for transradial amputees. The proposed design has an innovative load-transferring mechanism to modulate the joint stiffness for handling objects with different weights. The wrist joint is built with a 3D printer from ABS material and employs a brushless DC motor for joint stiffness modulation. The prototype of the RoboWrist is characterized for the stiffness variation in handling different weighed objects, and its functional evaluation is presented with a case study. We showed changing stiffness for different load settings, i.e., light, medium, and stiff settings. The real-time functional evaluation of RoboWrist shows success in handling objects with different weights.

3.1 Method

A 2-DoF wrist joint capable of preconditioning the stiffness of the wrist joint according to the object being held by the hand prosthesis is described. The innovative design of this wrist prosthesis allows it to be compact, and using 3D printing and ABS materials results in a lightweight prosthesis. Static structural analysis based on the maximum of 5 kg load is implemented. Additionally, a simulation to determine wrist joint stiffness is discussed in this section.

3.1.1 Conceptual Design and CAD modeling

Even though the human wrist joint has 3-DoF, it can be considered as a 2-DoF joint that performs F/E and R/U deviation movements to achieve the function in the simplest manner. 3rd DoF would be achieved through the forearm by the elbow joint. The prosthetic wrist should be able to replicate these movements to function similarly to the human wrist joint [56]. Therefore, the RoM for these movements should be determined based on functional movements of the human hand and wrist, which are from $-54°$ to $48°$ for F/E and from $-22°$ to $38°$ for R/U movements. The dimensions of the wrist prosthesis are determined according to the anthropomorphic measurements of the human body [57]. According to the desired movements, the proposed design has two parts: the rotating part and the base part. The base part is connected to the housing of the DC Motor. The rotating part is connected to the hand prosthesis and rotates on the base part through a spherical joint. Due to the geometrical constrain in design, the spherical joint allows the joint to rotate in two planes. The interaction between these two components is crucial in determining the RoM during movements. The RoM is governed by specific geometric constraints that regulate the articulation of the wrist joint. Notably, tendons originating from the pulley on the DC motor's shaft pass through the pulleys inside the base part and are fixed on the rotating part. As a result, when a load is applied to the wrist joint, the rotating part can rotate within the spherical part of the base, facilitating smooth and controlled movements. Fig. 10 shows the CAD model of the rotating and base parts. Also, in this figure, R/U and F/E movements are depicted.

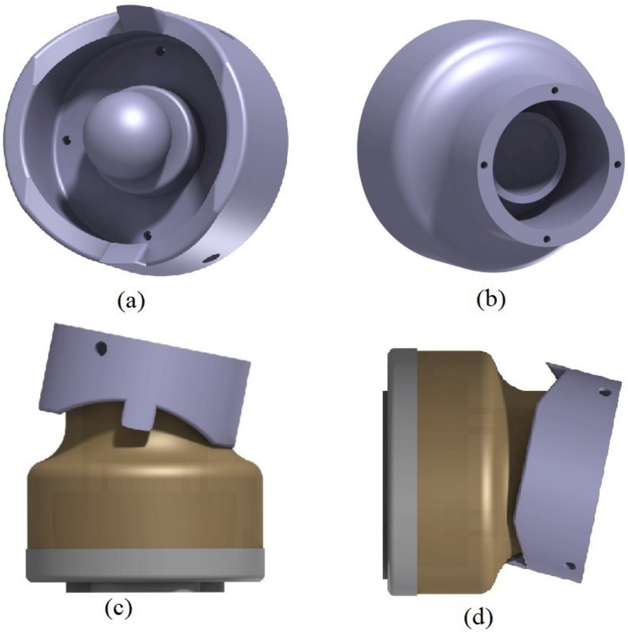

Figure 10: The CAD model of the rotating part (a), the CAD model of the base part(b), Ulnar deviation of the rotating part on the base part (c), Flexion movement of the rotating part on the base part (d)

As it is seen in Fig. 10 (c,d), the geometrical constraints on the parts determine the F/E and R/U movements' RoM.

To vary the stiffness of the wrist joint, tendons are used, which pass through the base parts, and they are tensioned using a DC motor. To modulate the stiffness of the wrist joint through the tendons and DC motor, two sets of pulleys are used. While the role of the small pulleys is to change the direction of the tendons by 90° to be able to pass them directly from the big pulley, the role of the big pulley is to connect the motor to the base part to pull the tendons. Four small pulleys are located on the wrist base and connected to this part via plastic pins. Fig.11 shows the assembly of pulleys inside the wrist base part.

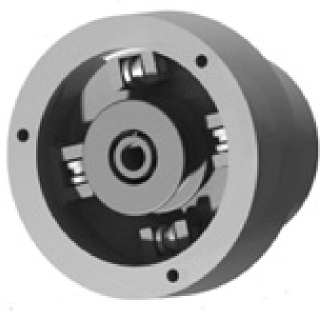

Figure 11: Assembly of pulleys inside the wrist base part

The housing part holding the DC motor and the base part is designed and assembled into other parts. Additionally, an apparatus is designed to hold the wrist joint and allow the able-bodied participants to perform the experimental evaluation, as shown in Fig.12.

Figure 12: The CAD model of the apparatus

Fig. 13 and Table 10 show the exploded view and bills of material (BOM) of the wrist joint.

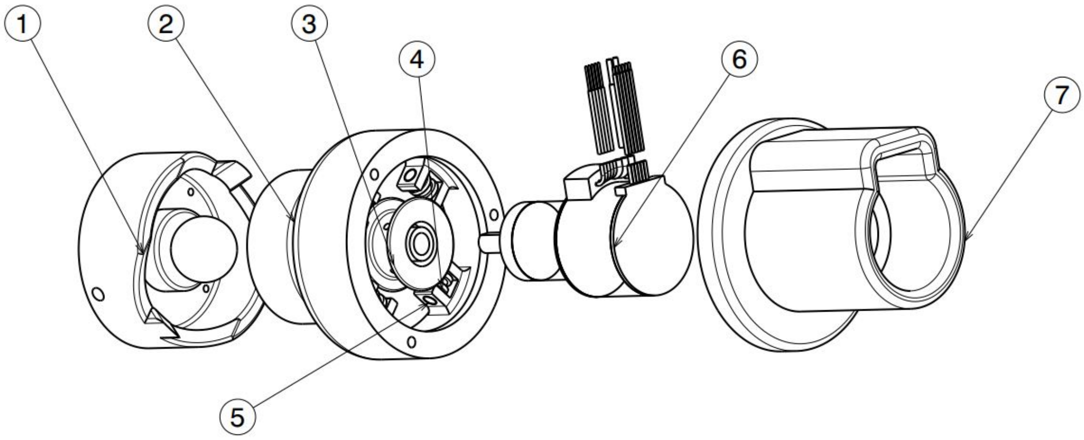

Figure 13: Exploded view of the wrist joint

Table 10: Bills of the material of the wrist joint

Part Number	Part Name	Quantity
1	Wrist Joint	1
2	Base of the joint	1
3	Big Pulley	1
4	Small Pulley	4
5	Pins of Small Pulleys	4
6	Motor and Gearbox	1
7	Motor Housing	1

This design mimics the human wrist joint's motion in two planes while maintaining stability and functionality in the wrist joint's operation. By carefully considering the geometrical relationships between the rotating and base parts, which are provided by the physical limits in the design, this mechanism achieves the desired RoM for enhanced performance and usability in diverse applications.

3.1.2 Structural Analyses

This section describes the structural analyses for the RoboWrist design. The static loads during the different tasks are analyzed, and maximum deflection and stresses are determined using ANSYS. The most dominant stresses on the wrist joint are assumed to be the applied bending and shear stresses from the grasped object. The bending moment is applied in two planes (R/U deviation and F/E movements), and the resultant stress should be calculated for these two planes. The bending moment is calculated as,

$$\vec{M} = \vec{r} \times \vec{F} \tag{9}$$

where $\vec{F}$ is the force vector, which is the weight of the held object and the hand prosthesis, and $\vec{r}$ is the moment arm vector, which is the position between the center of mass of the object and wrist joint connected part to the hand prosthesis, respectively. Thus, the maximum stress in the wrist joint can be calculated while the hand prosthesis holds a $5kg$ (set as the maximum mass of the commonly used objects during ADL) object according to the dimensions of the prosthesis. Since we are looking for a low-weight material to be strong enough against the applied stresses, we used the Ashby diagram to confirm the ABS material. Following that, we implement structural analysis in ANSYS with the exact shape of the wrist joint to obtain the maximum stress and maximum deflection in the wrist joint, as shown in Fig. 14 and 15.

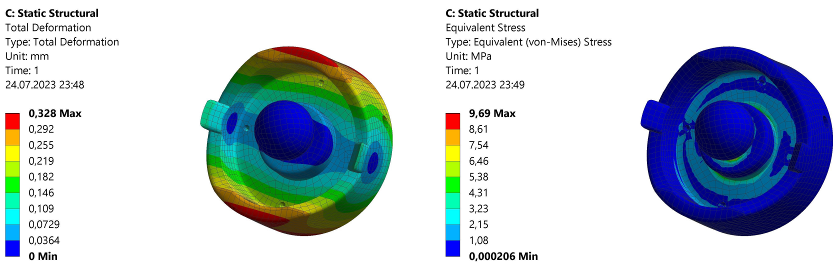

Figure 14: The total deflection (left) and Von-Mises stress (right) results for the R/U deviation in the wrist joint using ANSYS

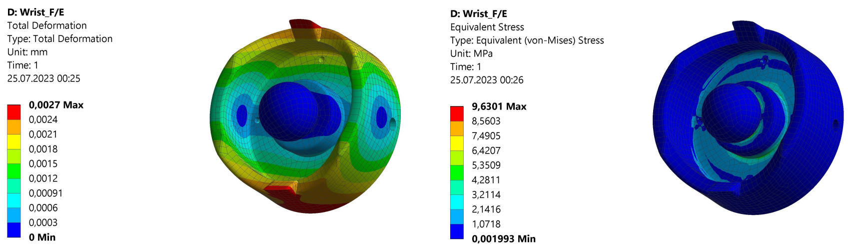

Figure 15: The total deflection (left) and Von-Mises stress (right) results for the F/E movement in the wrist joint using ANSYS

In these analyses, the wrist joint is kept fixed at its spherical part while the force and moment from the load are applied to the connected part of the joint for the hand prosthesis. As it is observed in Fig. 14, the maximum stress on the wrist joint is 9.69 MPa, and the maximum deflection is 0.33 mm for R/U deviation, while these values for F/E movements are 9.63 MPa and 0.003 mm.

3.1.3 Tendons selection

The fishing line made from Polyethylene (PE) with fiberglass reinforcement (30%) (AKAJIMA STEELEX, 0.4 mm) is used as tendons in the wrist prosthesis. The capacity of these fishing lines varies from 15 lb to 60 lb. Based on their module-strength chart, the strain at the yield point is approximately 2.75%. The calculations for the stiffness of the tendons are as follow,

$$\sigma = E\epsilon \tag{10}$$

$$F = \sigma A_0, F = k\Delta L \tag{11}$$

$$\epsilon = \frac{\Delta L}{L_0} \tag{12}$$

Where E, k, L_0, and ϵ are the Elastic module, stiffness, initial length, and strain of the fishing line. Therefore the stiffness of the fishing line is determined as,

$$k = \frac{EA_0}{L_0} \tag{13}$$

For a Polyethylene fishing line with a 0.4 mm diameter and length of 30 mm, the stiffness of this tendon is 0.67 $\frac{N}{mm}$.

3.1.4 Motor Selection

The maximum required velocity, torque, and power should be specified to select a proper motor for the wrist joint. Three parallel tendons on each side are employed in the wrist joint to make at least a stiffness of 2 N/mm. Therefore, according to the calculated stiffness and based on $\delta = F/k$, the deflection of the tendons is 12.5 mm. Also, the required velocity to bring the wrist joint from the lowest stiffness to the highest stiffness (based on user response time for a different project that is set to be 0.1 s) is 125 mm/s. Hence, considering a pulley around the shaft of the motor with a diameter of 10 mm, the motor velocity should be at least 120 rpm which is reachable in most DC motors, and it would not be a limitation parameter. The generated torque is determined according to the tendon force exerted by the applied load and the radius of the pulley as follows,

$$\vec{\tau} = \vec{r} \times \vec{F} \tag{14}$$

Where r and F are the position vector of the radius of the pulley and the vector of tendons force. Considering the maximum force on the tendons and the radius of the pulley, the required torque from the motor is calculated as 250 $mN.m$. The required power for the DC motor is calculated as follows,

$$P = \tau\omega \tag{15}$$

Where ω is the required angular velocity of the motor in rad/s. Considering the torque and velocity of the motor, the maximum required power for the current study is determined as 3.15 W. Considering the constraints imposed by motor torque and mass, the ideal motor for the given application should possess high continuous torque, a low reduction ratio, and a compact and lightweight design. A Faulhaber Flat DC motor featuring an external diameter of 32 mm, length of 16 mm, and mass of 65 g in combination with a planetary gearhead with a reduction ratio of 11 and mass of 66 g is selected. This motor not only fulfills the spatial limitations but also offers a rated torque of 37 mN.m with an efficiency of 84%.

3.1.5 Simulation of the wrist stiffness

In order to assess the stiffness of the wrist joint in a theoretical context, it is essential to establish the relationship between torque and F/E or R/U angle. This relationship can be formulated as a cross-product involving the moment arm and the force. The moment arm is determined by measuring the distance from the wrist joint to the center of mass (COM) of the hand prosthesis together with the applied load, while the force vector is defined as the applied load to the COM of the hand prosthesis. For this purpose, the quasi-static model is implemented in simulation. According to this model, the resulting components of the moment arm vector are defined as follows,

$$\vec{r} = d\cos\theta\hat{i} - d\sin\theta\hat{j} \tag{16}$$

Where d is the distance between the wrist joint and COM of the hand prosthesis. Also, the applied load is defined as,

$$\vec{F} = -mg\hat{j} \tag{17}$$

Where m is the total mass of the hand prosthesis and applied load. Therefore, the torque is as follows,

$$\vec{\tau} = -mgd\cos\theta\hat{k} \tag{18}$$

Fig. 16 shows the schematic of the wrist joint deviation for F/E motion.

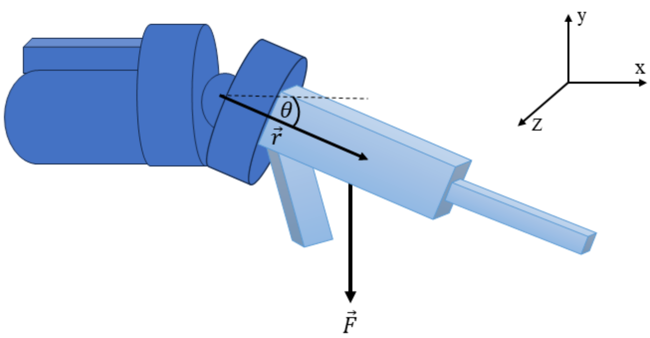

Figure 16: The schematic of the wrist joint deviation when applying load

Based on the functional RoM, the wrist joint stiffness is determined by torque angle relation. Various masses are considered when the F/E and R/U angles change from zero to 54°. Fig. 17 shows the behavior of the wrist joint against multiple masses theoretically. In this simulation, the load is constant, while the wrist angle varies based on the functional RoM.

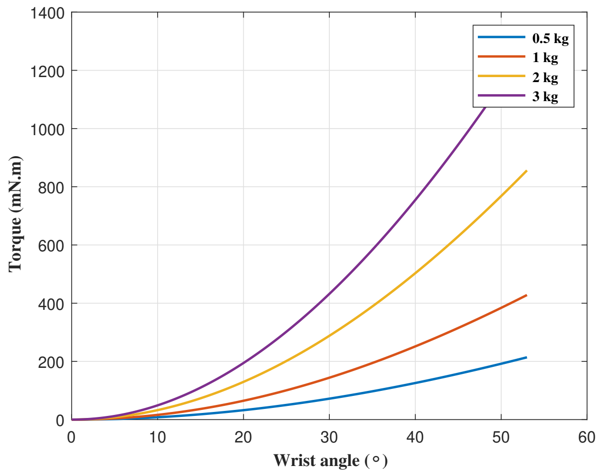

Figure 17: torque-angle relation of the proposed wrist joint

In Fig. 17, the blue, red, yellow, and purple lines represent the torque-angle relation of the wrist joint under 500 g, 1000 g, 2000 g, and 3000 g loads, respectively. To evaluate the wrist joint stiffness under different load settings, the torque-angle relation in this figure is considered. The stiffness values of the wrist joint are approximated by a linear fit as 5.27 $mN.m/deg$, 10.98 $mN.m/deg$, 21.98 $mN.m/deg$, and 32.98 $mN.m/deg$ for the 500 g, 1000 g, 2000 g, and 3000 g loads, respectively.

3.2 Prototyping

The wrist prosthesis is manufactured from ABS material using an Ultimaker 2^+ 3D printer. The infill of the printing is considered as 40%, and a nozzle with a diameter of 0.4 mm is used for prototyping. Fig. 18 shows the final prototype of the wrist joint.

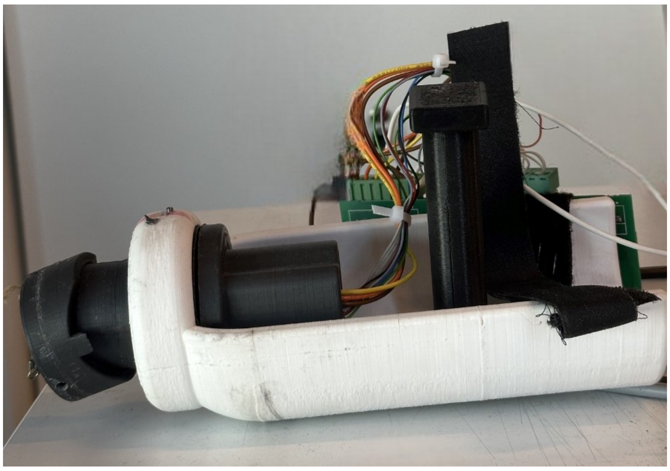

Figure 18: 2-DoF wrist prosthesis prototype

The overall mass of the prosthesis is 144 g, including the housing part, and the volume of the RoboWrist prosthesis is $110 \times 64 \times 64mm$, and the writ joint dimensions are $24 \times 54 \times 54mm$ which is very close to the average of human wrist size (52 mm) [57]. The proposed wrist prosthesis is connected to the HandMECH as a hand prosthesis to perform the tasks. A PCB is designed to connect the motor and the sensors to the driver in safe mode, and the motor driver is mounted on it.

3.3 Experimental evaluation of RoboWrist

In this section, two main experimental evaluations are conducted with the 2-DoF wrist prosthesis. The stiffness characterization evaluations of the wrist joint for F/E and R/U deviation movements are performed to approximately illustrate joint stiffness change according to different loads. Additionally, a functional evaluation of RoboWrist is performed with 20 participants to determine the system's performance for handling bottles with different weights.

3.3.1 Wrist Prosthesis characterization

In order to illustrate the stiffness of the wrist joint, four distinct settings are adopted. These settings encompass varying stiffness levels, ranging from light to medium-light, medium, and stiff. Each setup entails the inclusion of a specific mass that is intended to be carried by the wrist joint. The torque necessary to support the applied weights is identified as follows,

$$\tau_l = mgl_c \tag{19}$$

The l_c is the COM of the hand prosthesis together with the applied force. Also, the torque calculation is considered a friction coefficient of 0.37 between two ABS parts as τ_f based on a study by Slavkina1 and Lopatina [58]. The torque of the motor is determined as follows,

$$\tau_m = \frac{(\tau_l + \tau_f)}{Nr} \tag{20}$$

N and r are the gearbox's reduction ratio and the big pulley's radius, respectively. The reduction ratio of the gearbox is 11, and the pulley radius is 10 mm. Since the input of the controller system is the current of the motor, the calculated torque is converted to current as follows,

$$I = k_I \tau_m \tag{21}$$

Where k_I is the motor's torque constant, taken from the motor's datasheet as $k_I = 0.07A/mN.m$. The applied masses for each setting and the required current for each one are listed in Table 11.

Table 11: The properties of different wrist stiffness settings

Setting name	Applied Mass (g)	Required Current (mA)
Light	500	353
Medium Light	1000	707
Medium	2000	1415
Medium Stiff	3000	2123
Stiff	4000	2830

According to Table 11, for each setting, the RoboWrist is brought to the zero angle, and the corresponding current is set via Fualhaber Motion Manager software and applied to the motor. To approximate the joint stiffness of the RoboWrist for each setting, 18 masses with 100 g incremental increase from 300 g to 2000 g are applied to the hand prosthesis. The reason why over 2000 g is not applied is due to the cut-off frequency of the motor that is acquired during the experiment. The resulting angle of the wrist joint is then measured using an IMU sensor (BNO055 9-DoF Absolute Orientation IMU), as depicted in Fig. 19. The stiffness of the wrist joint for different settings is then approximated by calculating the torque exerted by weights on the hand prosthesis (using Eq. 22) and plotting the wrist joint's torque against the measured joint angle.

$$\tau_w = mgl_c \cos\theta \tag{22}$$

Where τ_w and θ are the wrist torque and angle, respectively. Fig. 19 shows the setup for joint stiffness characterization of the proposed 2-DoF wrist prosthesis for F/E and R/U deviation motions.

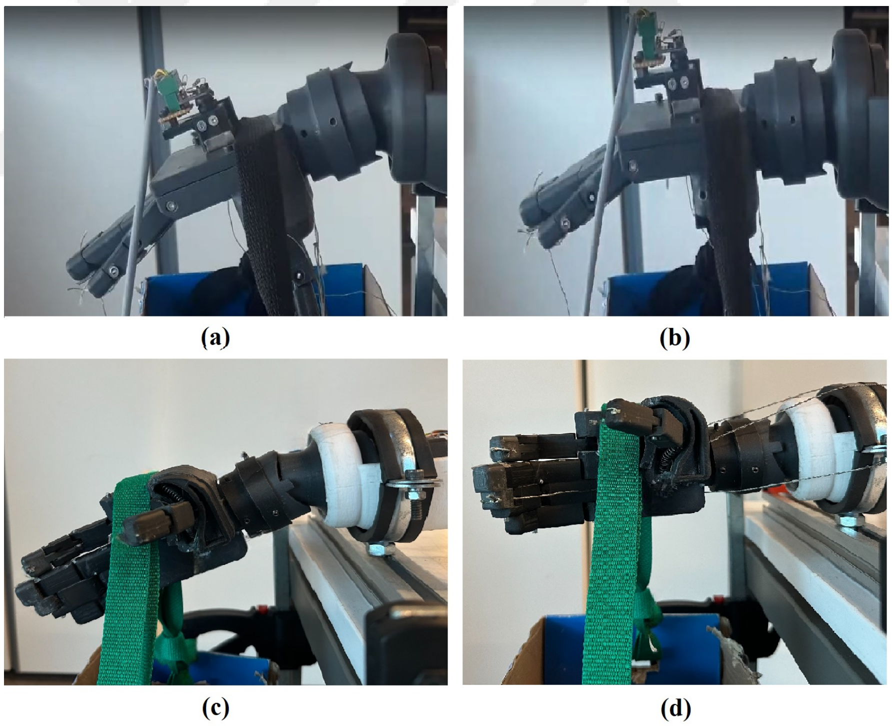

Figure 19: Experimental characterization of the wrist joint for F/E movement (Top): compliant (Left), stiff (Right) and Experimental characterization of the wrist joint for R/U deviation (bottom): compliant (Left), stiff (Right)

In Fig. 20, the experimental results of the wrist joint characterization for F/E movement are plotted for four modes of presetting conditions.

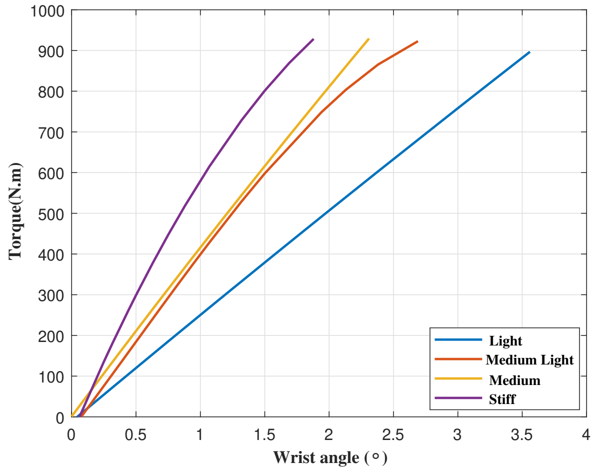

Figure 20: Experimental characterization results of the wrist joint for F/E motion

Fig. 20 shows the calculated torque (Eq. 22) and the measured joint angles based on the applied masses for each setting of F/E movement. Also, the wrist joint stiffness is illustrated by this figure. The blue, red, yellow, and purple lines represent the different settings as light, medium light, medium, and stiff, respectively. The stiffness of the wrist prosthesis is determined as 252 $mN.m/deg$ for the light setting, 398 $mN.m/deg$ for the medium light setting, 406 $mN.m/deg$ for the medium setting, and 575 $mN.m/deg$ for the stiff setting. Fig. 21 shows the experimental characterization results of the wrist joint for R/U movement, plotted for the four settings of presetting conditions.

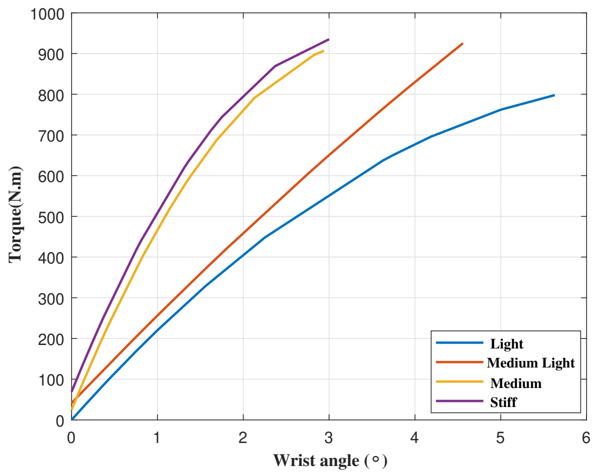

Figure 21: Experimental characterization results of the wrist joint for R/U deviation

In Fig. 21, the blue, red, yellow, and purple lines represent the different settings as light, medium light, medium, and stiff for the R/U deviation of the wrist joint, respectively. The stiffness of the RoboWrist in this deviation is determined as 177 $mN.m/deg$ for the light setting, 203 $mN.m/deg$ for the medium light setting, 406 $mN.m/deg$ for the medium setting, and 425 $mN.m/deg$ for the stiff setting.

The finite element method (FEM) analyses show that the wrist joint is strong enough while a 5-kg load is applied to the wrist joint when it is fixed and rigid. To evaluate the load-carrying capacity of the wrist joint with a pre-conditioned torque without failing, loads of 3.3 kg and 4.4 kg are applied to the wrist joint while a current of 2100 mA is supplied to the motor. The task is failed when the RoboWrist prosthesis is not able to hold the object and the motor is cut off. In this evaluation, These loads are applied as a single load without incremental increasing of the mass. The resulting deviation of the wrist joint is measured as yielding an average joint angle deviation of 9.14° and 18.11° for the 3.3 kg and 4.4 kg loads, respectively. In the case of a 4.4 kg load, the motor is cut-off, and the RoboWrist cannot hold the object and reaches its maximum deviation limit.

3.3.2 Functional evaluation

As part of the project to evaluate the Algorithm for the EEG system, light (half water bottle) and heavy settings (1-liter water bottle) tests are conducted on healthy individuals. These evaluations are approved by the Clinical Research Ethics Committee of Erciyes University with document number 2019/32. In order to make sure both the hand and wrist prostheses maintain a firm grip on objects without any deviation in joint angles, the position control of the wrist joint is conducted before performing the functional tests. Hence, reference values are established for the joint angle deviation and the angular velocity of the wrist prosthesis, following a constant function that brought the prosthesis to zero. An inverse quasi-static model with a PD controller is employed to calculate the required current to be transmitted to the motor to achieve the desired position. By utilizing the measured joint angle (q) and angular velocity ($\dot{q}$) of the wrist joint and computing the errors between the desired angle/velocity and the measured values, the current is applied to the actuator based on the PD controller and inverse model. The desired position is tracked by tuning the P and D gains. The block diagram of the designed control system for the wrist joint is depicted in Fig. 22.

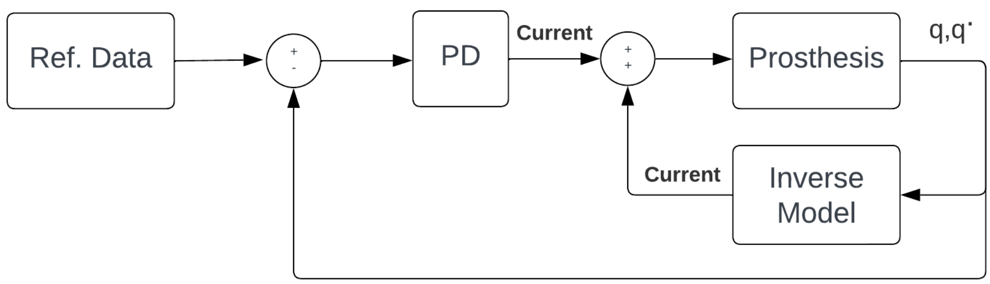

Figure 22: Block diagram of the control system

In order to control the stiffness of the prosthesis, the computed torque method, designed in MATLAB/Simulink environment, is implemented into the prosthesis using an Arduino Uno microcontroller. The signals are sent to the motor as PWM signals through the serial connection. The position control of the wrist prosthesis is carried out under two conditions: when there is only a hand prosthesis and when an external load of one kilogram is applied. The results of these tests are depicted in Fig.23 and 24.

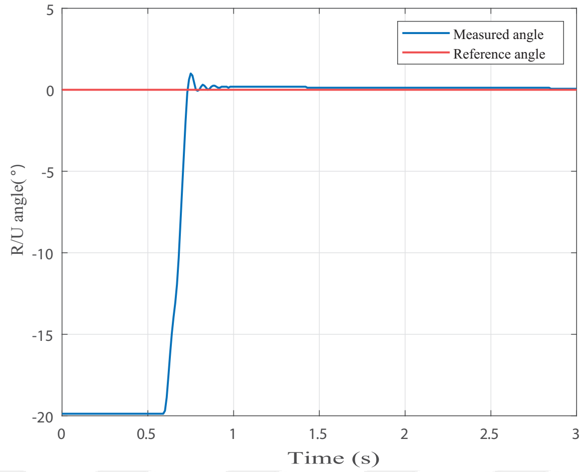

Figure 23: The wrist prosthesis position control when there is no load on the hand prosthesis

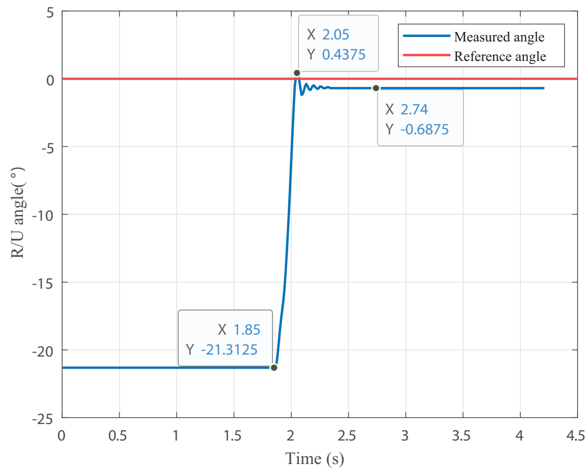

Figure 24: The wrist prosthesis position control when there is 1kg load on the hand prosthesis

As shown in Fig. 23 and 24, the currents are applied at 1.85 s, and 0.6 s for hand prosthesis weight and extra load conditions. The deviation angles in the wrist joint at the beginning of the tests are 20°, 21.31° for the hand prosthesis weight and extra load conditions. The wrist prosthesis is able to track the reference position in 0.15 s for hand prosthesis weight load and 0.2 s when there is a 1 kg load on the hand prosthesis. The time of the tracking is calculated when the task starts. A steady state error of 0.12° and 0.68° is observed for hand prosthesis weight and 1 kg additional mass cases, respectively.

To evaluate the algorithm for the EEG system, 20 participants take part, comprising 15 men and five women, with a mean age of 27.6±4.64. Initially, the participants are equipped with hand and wrist prostheses (HandMECH and RoboWrist prostheses). The Bowden Cable mechanism generates the force exerted in the fingers of the hand, and individual adjustments are made to the cables' stretching to apply force using the opposite shoulder. To familiarize themselves with the prosthesis, the subjects must be ready by holding and lifting a half-full and full water bottle 5 minutes before commencing the tests.

During each experiment, a series of images depicting half-filled and full bottles are presented on a screen, with the order of these images randomized throughout the tests. The participants are instructed to lift and lower the bottles in response to these visual cues as depicted in Fig.25.

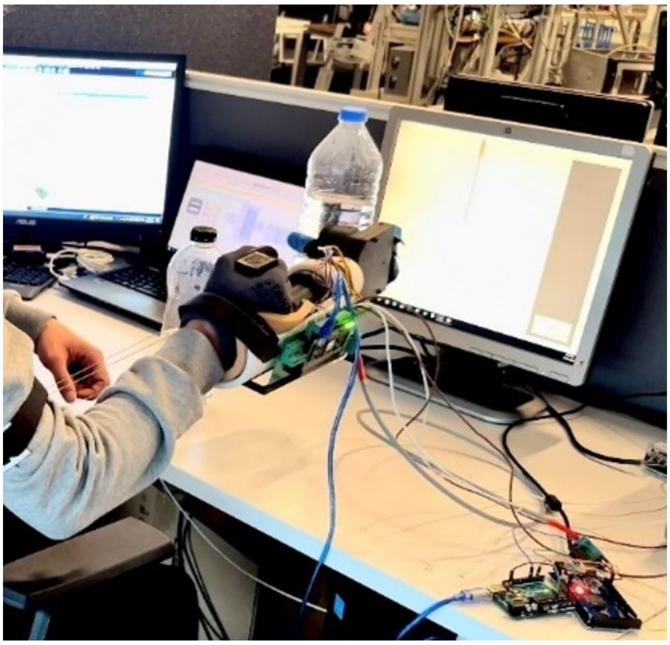

Figure 25: The experiment environment of functional tests for wrist prosthesis

Within the experimental setup, each individual performed 15 lifting and lowering with various bottle options. Three data sets are recorded in these experiments, including brain signals, input current to the motor from the control system, and output current from the motor. Based on a safety factor of 1.41 and considering a half-filled bottle weighing 500 g and a full bottle weighing 1 kg, the current required to lift each bottle is 500 mA and 1000 mA. Since the motor's driver utilizes PI torque control, the analog signal sent is adjusted to ensure that the motor's current output matches the required values of 500 mA and 1000 mA. During sending the analog signal through the driver of the motor, it uses filters to make these signals noiseless, but these filters can delay the response time of the result. As shown in Fig. 26, when this filter is set at 4000 μs, the delay for the motor current to decrease from 1000 mA to 500 mA is observed as 10 s.

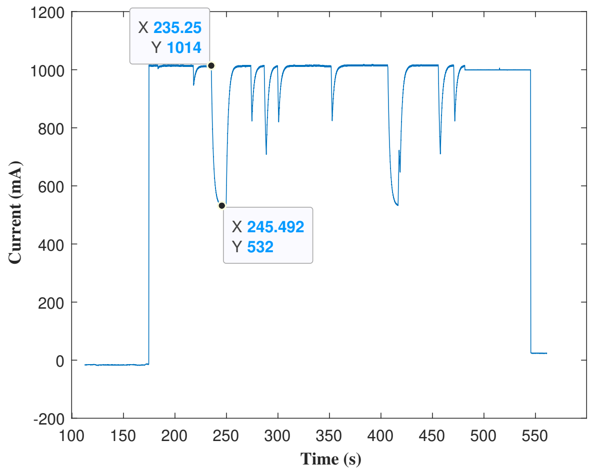

Figure 26: The delay of the motor's current response to the input signal when the filter is set 4000 μs

Achieving a balance between oscillation and delay time is crucial, as reducing the filter value resulted in motor torque oscillations but reduced the overall time delay. To address this trade-off, the filter value is adjusted to 140 μs in order to approach a desired reaction time of 0.1 s, while the motor's actual reaction time is measured to be 0.29 s. The torque oscillation in the motor due to the reduced filter value is observed to be 0.79 mNm, as depicted in Fig. 27. This amount corresponds to 5.49% of the maximum torque and falls within an acceptable range.

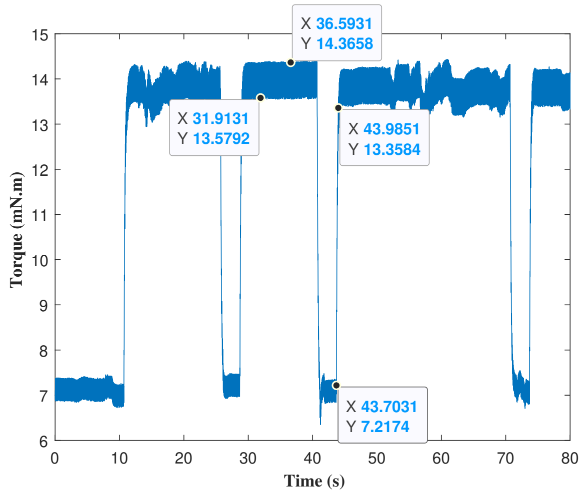

Figure 27: The delay of the motor's current response to the input signal when the filter is set 140 μs

According to this figure, it lasts 0.29 s for the demanded torque of the motor to reach the requested torque, and there is a 0.19 s delay in the motor response to the input current. Additionally, in Fig. 28 the tracking of the requested torques by the demanded torques to the motor in real-time control is shown.

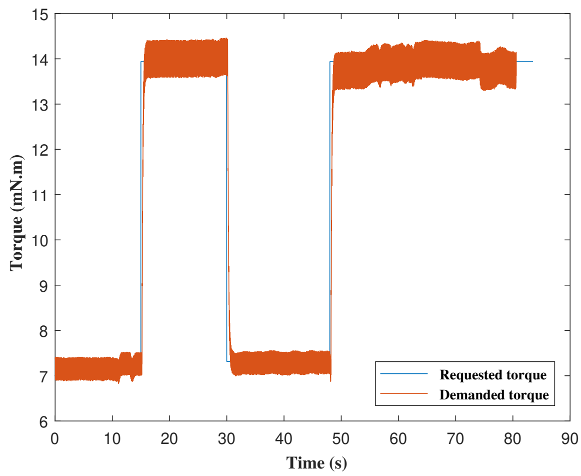

Figure 28: The input and output signal of the motor

In this figure, the red line represents the demanded torque of the motor, while the blue line depicts the requested torque based on the input signal received from the EEG system. According to this figure, the demanded torque tracks the requested torque exactly and shifts to the new value during all tests when the input signal changes. The real-time signal from the EEG system is seamlessly transferred to the prosthesis. During the experimental evaluations, the motor correctly responds to different input signals corresponding to tasks involving both light and heavy objects.

3.4 Discussion

The structural analysis results for the rotating part show that the designed part, manufactured from ABS material, is strong enough to hold a 5 kg load based on the mechanical properties of the material. This load can be held by the wrist with fixing it manually to a rigid mode. Hence, the wrist stiffness in this mode equals to the material stiffness used in manufacturing. The total mass of the RoboWrist, including the actuation system, is 290 g, which is 58% lighter than [59], while the body of the wrist, excluding the actuation system, is 144 g. The diameter of the wrist joint is 54 mm, which is 2% less than the average diameter for human wrist [60]. Therefore, the compactness of the design of RoboWrist is achieved with a negligible difference. Using plastic material such as ABS instead of metal in prototyping the RoboWrist reduces the overall mass. Further reduction would be achieved by optimizing the geometry, i.e., topology optimization, and using different materials. Additionally, selecting an optimized infill for the printing can reduce the overall mass of the RoboWrist. Moreover, implementing design optimization based on the functionality of the parts can also reduce the mass of the RoboWrist.

To assess the stiffness behavior of the wrist joint prosthesis, a characterization of its stiffness is conducted for different settings by applying the corresponding required current to the motor. The required torque for each setting is determined based on the applied loads on the prosthesis (through Eq. 22). According to the results of the RoboWrist characterization, increasing the pre-conditioned torque value in the wrist joint causes an increase in the stiffness of the wrist joint. Notably, the light setting exhibited the lowest stiffness, while the stiff mode displayed the highest stiffness for both F/E movement and R/U deviation. Since the applied current to the motor for the pre-conditioned currents of more than 2100 mA decreases after 5 s during the tests, it is not possible to provide a current of more than this value on the motor. The Robowrist is designed to hold a 5-kg load during the stiffness characterization. Although it can hold this load while fixing to a rigid mode, the characterization evaluation is performed for a maximum of 3.3 kg load (66% of the designed load). Slipping the pulley (inside the base part) with respect to the motor's shaft would decrease the provided torque by the actuation system. Additionally, the backlash of the system can also reduce the efficiency of the actuation system. Hence, the high stiffness value that can be achieved would be reduced. Moreover, efforts can be made to reduce friction between the wrist joint components to achieve the highest level of stiffness in the wrist joint, which is not attainable due to the motor's cut-off. Since the main friction in the wrist joint is between the base and the rotating parts, the printing quality of these two parts can increase the friction between them. Therefore, enhancing the quality of prototyping makes the desired goals of the study more achievable. Additionally, refining the tendons' route inside the joint would reduce the resultant friction. Moreover, geometrical refining, i.e., smoothing the shapes to reduce the contact area, can also improve the accessibility to higher stiffness levels. As a result of decreasing the motor torque during the evaluations, differences in wrist joint stiffness in R/U deviation between the light, medium-light, and medium characterization settings are more significant compared to the stiffness difference between medium and stiff modes. The maximum wrist joint stiffness in the F/E movement is 575 $mN.m/deg$, whereas the maximum wrist joint stiffness is 425 $mN.m/deg$ for R/U deviation. The variance in stiffness between F/E and R/U deviation movements is due to the approximation of the stiffness based on their RoM. It must be noted that the stiffness of the proposed RoboWrist can vary continuously from the stiffest mode to the most compliant mode, but to illustrate the stiffness characterization of the prosthesis, different settings are presented.

The characterization of the wrist joint shows that the deviation in the wrist joint for loads with a 100g incremental increase from 300 g to 2 kg (which covers most of the daily handled objects) varies in an acceptable range. On the other hand, according to the results, the RoboWrist can carry a maximum mass of 3.3 kg with 9.14° deviation in the wrist joint, which can be improved by decreasing the friction and backlash in the system.

The functional evaluations of the RoboWrist show the RoboWrist can hold and carry a 1-liter bottle (which can be considered a commonly heavy object in ADL). Additionally, the implemented control method on the system can respond to all the requested tasks from the EEG system correctly with a maximum delay of 0.19 s. Despite configuring the response time to be 0.1 seconds, the functionality of the RoboWrist in carrying out tasks is unaffected by this delay, as demonstrated in the supplementary video. To improve transient response and decrease the delay of the system, other control methods, such as Lead-Lag compensator, can be implemented.

CHAPTER IV

CONCLUSIONS

This study presents the design and evaluation of a lightweight and biomechanically inspired body-powered hand prosthesis for individuals with upper limb amputations. The prosthesis is specifically designed to mimic the natural movements of fingers and thumb, enabling it to perform various tasks encountered in daily activities. The overall mass of the prosthesis is 168 g, which makes it lighter than the existing body-powered hand prosthesis, and it can pick and place objects of 1kg. The unique 3D trajectory for the thumb realizes most of the tasks during the experiments and gives better control of holding the objects to the amputee while it decreases the required DOF for the HandMECH. The triple fingers make the prosthesis lighter and less complex. The designed hand prosthesis is evaluated using established test procedures, including the BBT and the SHAP test. The results demonstrate the prosthesis's functionality and comparative advantage over similar hand prostheses. These findings highlight the potential of the developed hand prosthesis to enhance the quality of life for individuals with upper limb amputations. Further improvements and refinements based on user feedback and additional performance evaluations will be implemented in future iterations of the prosthesis. It is already planned to improve the design of the prosthesis with topology optimization to decrease the mass and also to improve the thumb motion efficiency and its control. Friction should also be reduced in joint levels and tendon routing design and should be optimized for better gripping performance. Furthermore, the design should be refined for the best quality of 3D printing to achieve a near-product level. On top of that, the experiments with amputees would serve to evaluate the functionality and user-acceptance of the HandMECH for further improvement and eventually achieving the final product.

Additionally, in this thesis, a 2-Dof variable stiffness wrist joint is proposed. The proposed 2-DOF wrist prosthesis, which utilizes a novel design for transmitting motor torque to the wrist stiffness, is capable of handling objects with different masses. By characterizing the wrist prosthesis, it is determined that the stiffness of the wrist joint can vary according to the applied forces. The functional tests with the proposed prosthesis exhibit successful responsiveness to all conditions, from the lightest to the stiffest. Furthermore, this lightweight (144 g) and functional wrist prosthesis holds the potential for use by a wide range of individuals with transradial amputations. Since the amputee individuals are the end-user of this prosthesis, the same experimental evaluations should be conducted with amputee participants to evaluate their acceptance and ease of use.

REFERENCES

[1] C. L. McDonald, S. Westcott-McCoy, M. R. Weaver, J. Haagsma, and D. Kartin, "Global prevalence of traumatic non-fatal limb amputation," *Prosthetics and orthotics international*, p. 0309364620972258, 2021.

[2] K. Ziegler-Graham, E. J. MacKenzie, P. L. Ephraim, T. G. Travison, and R. Brookmeyer, "Estimating the prevalence of limb loss in the united states: 2005 to 2050," *Archives of physical medicine and rehabilitation*, vol. 89, no. 3, pp. 422–429, 2008.

[3] D. S. Childress, "Historical aspects of powered limb prostheses," *Clin Prosthet Orthot*, vol. 9, no. 1, pp. 2–13, 1985.

[4] R. J. Schwarz and C. Taylor, "The anatomy and mechanics of the human hand," *Artificial limbs*, vol. 2, no. 2, pp. 22–35, 1955.

[5] L. Resnik, S. Ekerholm, M. Borgia, and M. A. Clark, "A national study of veterans with major upper limb amputation: Survey methods, participants, and summary findings," *PloS one*, vol. 14, no. 3, p. e0213578, 2019.

[6] L. V. McFarland, S. L. Hubbard Winkler, A. W. Heinemann, M. Jones, A. Esquenazi, *et al.*, "Unilateral upper-limb loss: satisfaction and prosthetic-device use in veterans and servicemembers from vietnam and oif/oef conflicts," *J Rehabil Res Dev*, vol. 47, no. 4, pp. 299–316, 2010.

[7] E. Biddiss, D. Beaton, and T. Chau, "Consumer design priorities for upper limb prosthetics," *Disability and rehabilitation: Assistive technology*, vol. 2, no. 6, pp. 346–357, 2007.

[8] E. A. Biddiss and T. T. Chau, "Upper limb prosthesis use and abandonment: a survey of the last 25 years," *Prosthetics and orthotics international*, vol. 31, no. 3, pp. 236–257, 2007.

[9] D. Datta, K. Selvarajah, and N. Davey, "Functional outcome of patients with proximal upper limb deficiency–acquired and congenital," *Clinical rehabilitation*, vol. 18, no. 2, pp. 172–177, 2004.

[10] C. R. Gambrell, "Overuse syndrome and the unilateral upper limb amputee: consequences and prevention," *JPO: Journal of Prosthetics and Orthotics*, vol. 20, no. 3, pp. 126–132, 2008.

[11] K. Østlie, R. J. Franklin, O. H. Skjeldal, A. Skrondal, and P. Magnus, "Musculoskeletal pain and overuse syndromes in adult acquired major upper-limb amputees," *Archives of physical medicine and rehabilitation*, vol. 92, no. 12, pp. 1967–1973, 2011.

[12] M. Sardelli, R. Z. Tashjian, and B. A. MacWilliams, "Functional elbow range of motion for contemporary tasks," *JBJS*, vol. 93, no. 5, pp. 471–477, 2011.

[13] F. Montagnani, M. Controzzi, and C. Cipriani, "Is it finger or wrist dexterity that is missing in current hand prostheses?," *IEEE Transactions on Neural Systems and Rehabilitation Engineering*, vol. 23, no. 4, pp. 600–609, 2015.

[14] B. Morrey, L. Askew, and E. Chao, "A biomechanical study of normal functional elbow motion.," *JBJS*, vol. 63, no. 6, pp. 872–877, 1981.

[15] M. Doğan, M. Koçak, Ö. O. Kılınç, F. Ayvat, G. Sütçü, E. Ayvat, M. Kılınç, Ö. Ünver, and S. A. Yıldırım, "Functional range of motion in the upper extremity and trunk joints: Nine functional everyday tasks with inertial sensors," *Gait & posture*, vol. 70, pp. 141–147, 2019.

[16] F. Cordella, A. L. Ciancio, R. Sacchetti, A. Davalli, A. G. Cutti, E. Guglielmelli, and L. Zollo, "Literature review on needs of upper limb prosthesis users," *Frontiers in neuroscience*, vol. 10, p. 209, 2016.

[17] G. Smit and D. H. Plettenburg, "Comparison of mechanical properties of silicone and pvc (polyvinylchloride) cosmetic gloves for articulating hand prostheses.," *Journal of Rehabilitation Research & Development*, vol. 50, no. 5, pp. 113–117, 2013.

[18] N. E. Krausz, R. A. Rorrer, *et al.*, "Design and fabrication of a six degree-of-freedom open source hand," *IEEE Transactions on Neural Systems and Rehabilitation Engineering*, vol. 24, no. 5, pp. 562–572, 2015.

[19] X. Li, Q. Huang, X. Chen, Z. Yu, J. Zhu, and J. Han, "A novel under-actuated bionic hand and its grasping stability analysis," *Advances in Mechanical Engineering*, vol. 9, no. 2, p. 1687814016688859, 2017.

[20] B. Peerdeman, M. Valori, D. Brouwer, E. Hekman, S. Misra, and S. Stramigioli, "Ut hand i: A lock-based underactuated hand prosthesis," *Mechanism and machine theory*, vol. 78, pp. 307–323, 2014.

[21] D. A. Bennett, S. A. Dalley, D. Truex, and M. Goldfarb, "A multigrasp hand prosthesis for providing precision and conformal grasps," *IEEE/ASME Transactions on Mechatronics*, vol. 20, no. 4, pp. 1697–1704, 2014.

[22] R. W. Beasley and G. M. de Bese, "Upper limb amputations and prostheses," *Orthopedic Clinics of North America*, vol. 17, no. 3, pp. 395–405, 1986.

[23] P. Parker, K. Englehart, and B. Hudgins, "Myoelectric signal processing for control of powered limb prostheses," *Journal of electromyography and kinesiology*, vol. 16, no. 6, pp. 541–548, 2006.

[24] H. Herath, R. Gopura, and T. D. Lalitharatne, "Prosthetic hand with a linkage finger mechanism for power grasping applications," in *2017 IEEE Life Sciences Conference (LSC)*, pp. 304–307, IEEE, 2017.

[25] R. Unal and B. Toker, "A hand prosthesis," Oct. 11 2021. PCT/TR2021/051036.

[26] P. James Lipsey MS, A. Thomas, *et al.*, "Design and evaluation of voluntary opening and voluntary closing prosthetic terminal device," *Journal of rehabilitation research and development*, vol. 52, no. 1, p. 63, 2015.

[27] E. B. Brokaw, I. Black, R. J. Holley, and P. S. Lum, "Hand spring operated movement enhancer (handsome): a portable, passive hand exoskeleton for stroke rehabilitation," *IEEE Transactions on Neural Systems and Rehabilitation Engineering*, vol. 19, no. 4, pp. 391–399, 2011.

[28] S.-y. Jung, S.-k. Kang, and I. Moon, "Design of biomimetic hand prosthesis with tendon-driven five fingers," in *2008 2nd IEEE RAS & EMBS International Conference on Biomedical Robotics and Biomechatronics*, pp. 895–900, IEEE, 2008.

[29] G. Smit, D. H. Plettenburg, and F. C. van der Helm, "The lightweight delft cylinder hand: first multi-articulating hand that meets the basic user requirements," *IEEE Transactions on Neural Systems and Rehabilitation Engineering*, vol. 23, no. 3, pp. 431–440, 2014.

[30] S. Cobos, M. Ferre, M. S. Uran, J. Ortego, and C. Pena, "Efficient human hand kinematics for manipulation tasks," in *2008 IEEE/RSJ International Conference on Intelligent Robots and Systems*, pp. 2246–2251, IEEE, 2008.

[31] S. Shimawaki, T. Murai, M. Nakabayashi, H. Sugimoto, *et al.*, "Measurement of flexion angle of the finger joint during cylinder gripping using a three-dimensional bone model built by x-ray computed tomography," *Applied bionics and biomechanics*, vol. 2019, pp. 1–9, 2019.

[32] K.-S. Lee and M.-C. Jung, "Three-dimensional finger joint angles by hand posture and object properties," *Ergonomics*, vol. 59, no. 7, pp. 890–900, 2016.

[33] N. M. Bajaj, A. J. Spiers, and A. M. Dollar, "State of the art in prosthetic wrists: Commercial and research devices," in *2015 IEEE International Conference on Rehabilitation Robotics (ICORR)*, pp. 331–338, IEEE, 2015.

[34] R. W. Schoenmarklin and W. S. Marras, "Dynamic capabilities of the wrist joint in industrial workers," *International Journal of Industrial Ergonomics*, vol. 11, no. 3, pp. 207–224, 1993.

[35] A. Bonebrake, J. Fernandez, R. Marley, J. Dahalan, and K. Kilmer, "A treatment for carpal tunnel syndrome: evaluation of objective and subjective measures.," *Journal of manipulative and physiological therapeutics*, vol. 13, no. 9, pp. 507–520, 1990.

[36] J. Aizawa, T. Masuda, T. Koyama, K. Nakamaru, K. Isozaki, A. Okawa, and S. Morita, "Three-dimensional motion of the upper extremity joints during various activities of daily living," *Journal of biomechanics*, vol. 43, no. 15, pp. 2915–2922, 2010.

[37] D. L. Nelson, M. A. Mitchell, P. G. Groszewski, S. L. Pennick, and P. R. Manske, "Wrist range of motion in activities of daily living," *Advances in the Biomechanics of the Hand and Wrist*, pp. 329–334, 1994.

[38] D. H. Gates, L. S. Walters, J. Cowley, J. M. Wilken, and L. Resnik, "Range of motion requirements for upper-limb activities of daily living," *The American journal of occupational therapy*, vol. 70, no. 1, pp. 7001350010p1–7001350010p10, 2016.

[39] R. G. Crowder, *Principles of learning and memory: Classic edition*. Psychology Press, 2014.

[40] G. M. Motis, "Artificial arm with stepped-up wrist drive and automatic wrist lock," vol. 5, pp. 3–12, May 19 1953. US Patent 2,638,604.

[41] J. Zajdlik, "The preliminary design and motion control of a five-fingered prosthetic hand," in *2006 International Conference on Intelligent Engineering Systems*, pp. 202–206, IEEE, 2006.

[42] J. L. Pons, E. Rocon, R. Ceres, D. Reynaerts, B. Saro, S. Levin, and W. Van Moorleghem, "The manus-hand dextrous robotics upper limb prosthesis: mechanical and manipulation aspects," *Autonomous Robots*, vol. 16, pp. 143–163, 2004.

[43] G. M. Motis, "Linear to rotational movement converter," *US Patent 2,638,604*, vol. 22, pp. 74–89, 1969.

[44] P. J. Kyberd, E. D. Lemaire, E. Scheme, C. MacPhail, L. Goudreau, G. Bush, and M. Brookeshaw, "Two-degree-of-freedom powered prosthetic wrist.," *Journal of Rehabilitation Research & Development*, vol. 48, no. 6, pp. 609–618, 2011.

[45] F. Montagnani, M. Controzzi, and C. Cipriani, "Preliminary design and development of a two degrees of freedom passive compliant prosthetic wrist with switchable stiffness," in *2013 IEEE International Conference on Robotics and Biomimetics (ROBIO)*, pp. 310–315, IEEE, 2013.

[46] D. Formica, M. Azhar, P. Tommasino, and D. Campolo, "A geometric framework for the estimation of joint stiffness of the human wrist," in *2019 IEEE 16th International Conference on Rehabilitation Robotics (ICORR)*, pp. 151–156, IEEE, 2019.

[47] M. Gabardi, M. Solazzi, D. Leonardis, and A. Frisoli, "Design and evaluation of a novel 5 dof underactuated thumb-exoskeleton," *IEEE Robotics and Automation Letters*, vol. 3, no. 3, pp. 2322–2329, 2018.

[48] K. Berning, S. Cohick, R. Johnson, L. A. Miller, and J. W. Sensinger, "Comparison of body-powered voluntary opening and voluntary closing prehensor for activities of daily life," *J Rehabil Res Dev*, vol. 51, no. 2, pp. 253–61, 2014.

[49] J. T. Belter, M. T. Leddy, K. D. Gemmell, and A. M. Dollar, "Comparative clinical evaluation of the yale multigrasp hand," in *2016 6th IEEE International Conference on Biomedical Robotics and Biomechatronics (BioRob)*, pp. 528–535, IEEE, 2016.

[50] V. Mathiowetz, G. Volland, N. Kashman, and K. Weber, "Adult norms for the box and block test of manual dexterity," *The American journal of occupational therapy*, vol. 39, no. 6, pp. 386–391, 1985.

[51] J. S. Cuellar, G. Smit, P. Breedveld, A. A. Zadpoor, and D. Plettenburg, "Functional evaluation of a non-assembly 3d-printed hand prosthesis," *Proceedings of the Institution of Mechanical Engineers, Part H: Journal of Engineering in Medicine*, vol. 233, no. 11, pp. 1122–1131, 2019.

[52] J. Zuniga, D. Katsavelis, J. Peck, J. Stollberg, M. Petrykowski, A. Carson, and C. Fernandez, "Cyborg beast: a low-cost 3d-printed prosthetic hand for children with upper-limb differences," *BMC research notes*, vol. 8, no. 1, pp. 1–9, 2015.

[53] L. Haverkate, G. Smit, and D. H. Plettenburg, "Assessment of body-powered upper limb prostheses by able-bodied subjects, using the box and blocks test and the nine-hole peg test," *Prosthetics and orthotics international*, vol. 40, no. 1, pp. 109–116, 2016.

[54] Y. Nemoto, K. Ogawa, and M. Yoshikawa, "F3hand ii: A flexible five-fingered prosthetic hand using curved pneumatic artificial muscles," in *2020 IEEE/SICE International Symposium on System Integration (SII)*, pp. 99–104, IEEE, 2020.

[55] J. Mouchoux, S. Carisi, S. Dosen, D. Farina, A. F. Schilling, and M. Markovic, "Artificial perception and semiautonomous control in myoelectric hand prostheses increases performance and decreases effort," *IEEE Transactions on Robotics*, vol. 37, no. 4, pp. 1298–1312, 2021.

[56] M. Rainbow, A. Wolff, J. Crisco, and S. Wolfe, "Functional kinematics of the wrist," *Journal of Hand Surgery (European Volume)*, vol. 41, no. 1, pp. 7–21, 2016.

[57] Z. Li, C.-C. Chang, P. G. Dempsey, L. Ouyang, and J. Duan, "Validation of a three-dimensional hand scanning and dimension extraction method with dimension data," *Ergonomics*, vol. 51, no. 11, pp. 1672–1692, 2008.

[58] V. Slavkina and Y. Lopatina, "Study of tribotechnical characteristics of 3d printed abs plastic samples," in *IOP Conference Series: Materials Science and Engineering*, vol. 963, p. 012032, IOP Publishing, 2020.

[59] N. A. Abd Razak, N. A. Abu Osman, H. Gholizadeh, and S. Ali, "Development and performance of a new prosthesis system using ultrasonic sensor for wrist movements: a preliminary study," *Biomedical engineering online*, vol. 13, pp. 1–14, 2014.

[60] S. Adewusi, M. Thomas, V. Vu, and W. Li, "Modal parameters of the human hand-arm using finite element and operational modal analysis," *Mechanics & Industry*, vol. 15, no. 6, pp. 541–549, 2014.

VITA

Mahsa Sarrafi Khosrowshah Graduated from Islamic Azad University in Iran in 2017. She started her master's program in mechanical engineering at Özyeğin University in 2020. She has worked in the Human-centered Design laboratory under the supervision of Dr.Ramazan Unal. Designing, developing, and evaluating body-powered hand and 2-DOF robotic wrist prostheses, in addition to designing and developing a pre-botic hand prosthesis, are her research experiences during her master's. Her fields of interest are biomechanical, hand and wrist prostheses, upper-body prostheses, control, and design.